Fourier Transform Infrared and Electron Spin Resonance Spectroscopic Studies of Model and Biological Membranes

PhD Thesis

Zoltán Kóta

Institute of Biophysics
Biological Research Centre
Hungarian Academy of Sciences
Szeged, Hungary

2003

To Mária, my wife, and to Kata, my daughter,
who fill my life with love

"God looked over everything he had made,
and saw that it was very good."
(Gen. 1.31.)

Contents

Abbreviations and Symbols

cDNA	Complementary DNA
Chl	Chlorophyll
DOPC	1,2-Dioleoyl-*sn*-glycero-3-phosphocholine
DPPC	1,2-Dipalmitoyl-*sn*-glycero-3-phosphocholine
DSC	Differential scanning calorimetry
DSPC	1,2-Distearoyl-*sn*-glycero-3-phosphocholine
ELIP	Early light-inducible protein
ESR	Electron spin resonance
FTIR	Fourier transform infrared
$\mathbf{H_{II}}$	Inverted hexagonal
GPAT	Glycerol-3-phosphate acyltransferase
IR	Infrared
LHCII	Chlorophyll a/b light harvesting antenna complex of photosystem II
MGDG	Monogalactosyl diacylglycerol
NMR	Nuclear magnetic resonance
$\boldsymbol{\nu_{as}CH_2}$	CH_2 antisymmetric stretching vibration
$\boldsymbol{\nu_{sym}CH_2}$	CH_2 symmetric stretching vibration
OSPC	1-Oleoyl-2-stearoyl-*sn*-glycero-3-phosphocholine
PG	Phosphatidylglycerol
5-SASL	5-(4',4'-Dimethyloxazolidine-*N*-oxyl)stearic acid spin-label
SDS PAGE	Sodium dodecyl sulfate polyacrylamide gel electrophoresis
SOPC	1-Stearoyl-2-oleoyl-*sn*-glycero-3-phosphocholine
SVD	Singular value decomposition
TEMPO	2,2,6,6,-Tetramethylpiperidine-1-oxyl
TOAR	Tobacco transformed with *Arabidopsis* cDNA for glycerol-3-phosphate acyltransferase
TOBA	Tobacco
TOSQ	Tobacco transformed with squash cDNA for glycerol-3-phosphate acyltransferase

$2A_{max}$	Hyperfine outer splitting
$2A_{min}$	Hyperfine inner splitting
D	$\nu_{sym}CH_2$ component assigned to disordered fatty acyl chain segments
f_i	Immobile fraction of 5-SASL
f_M	True membrane partition parameter of TEMPO
f_t	Approximate membrane partition parameter of TEMPO
K_r	Lipid-protein association constant
N_b	Number of lipid association sites of the protein
n_t	Total lipid/protein molar ratio
O	$\nu_{sym}CH_2$ component assigned to ordered fatty acyl chain segments
S	Order parameter
τ_R	Rotational correlation time

Publications

Papers related to the thesis

I. Droppa, M., Kóta, Z., Páli, T., Szalontai, B., Horváth, L. I., and Horváth, G.
Structural–functional organization of thylakoids in developing chloroplasts
In *The Chloroplasts: From Molecular Biology to Biotechnology,* eds. Argyroudi-Akoyunoglou, J. H., Senger, H. (Kluwer Academic Publishers), pp. 55–60., 1999

II. Kóta, Z., Szalontai, B., Droppa, M., Horváth, G., and Páli, T.
Fourier transform infrared and electron paramagnetic resonance spectroscopic studies of thylakoid membranes
J. Mol. Struct. **480–481**, 395–400, 1999

III. Kóta, Z., Debreczeny, M., Szalontai, B.
Separable contributions of ordered and disordered lipid fatty acyl chain segments to νCH_2 bands in model and biological membranes: A Fourier transform infrared spectroscopic study
Biospectroscopy **5**, 169–178, 1999

IV. Kóta, Z., Szalontai, B., Droppa, M., Horváth, G., and Páli, T.
The formation of an inverted hexagonal phase from thylakoid membranes upon heating
Cell. Mol. Biol. Lett. **7**, 126–128, 2002

V. Kóta, Z., Horváth, L. I., Droppa, M., Horváth, G., Farkas, T., and Páli, T.
Protein assembly and heat stability in developing thylakoid membranes during greening
Proc. Natl. Acad. Sci. USA **99**, 12149–12154, 2002

VI. Szalontai, B., Kóta, Z., Nonaka, H., and Murata, N.
Structural consequences of genetically engineered saturation of the fatty acids of phosphatidylglycerol in tobacco thylakoid membranes. An FTIR study
Biochemistry, In press

Other papers

I. Kóta, Z., Páli, T., and Marsh, D.
Orientation and lipid–peptide interactions of gramicidin A in lipid membranes: polarised ATR infrared spectroscopy and spin-label electron spin resonance
Submitted for publication

II. Csányi, L. J., Jáky, K., Dombi, Gy., Evanics, F., Dezső, G., and Kóta, Z.
Onium-decavanadate ion-pair complexes as catalysts in the oxidation of hydrocarbons by O_2
J. Mol. Cat. A **195**, 101–111, 2003

III. Csányi, L. J., Jáky, K., Kóta, Z., and Páli, T.
Oxidation of hydrocarbons by O_2 in the presence of onium salts and onium ion-pair complexes as catalysts
Submitted for publication

IV. Páli, T., Garab, G., Horváth, L. I., and Kóta, Z.
Functional significance of the lipid–protein interface in photosynthetic membranes
Submitted for publication

Chapter 1

Introduction

1.1 The importance of biomembranes

Membranes play a central role in both the structure and function of cells, therefore the study of biomembranes has become a meeting ground for a number of diverse scientific disciplines ranging from biophysics to molecular biology.

Biomembranes are multicomponent dynamic systems taking part in the regulation of a number of cell processes: they constrain the free diffusion of solutes and catalyse specific exchange reactions, which together determine the unique chemical compositions of the cellular and subcellular compartments; they store energy in the form of transmembrane ion and solute gradients and regulate the rate of energy dissipation; they provide an organizing matrix for the assembly of multicomponent metabolic pathways; and they govern the transfer of information between the compartments they separate by possessing ligand-specific receptors [1].

The major components of biological membranes are lipids and proteins, accordingly, these molecules are subject of extensive interdisciplinary research [2–7]. The fluid mosaic model [8] brought the mobility of membrane components into focus by conceptualizing the membrane as a sea of lipids in which embedded globular proteins are freely floating. The primary role of lipids is to provide the structural framework, whereas function is mostly carried by proteins. The mutual interactions of lipids and proteins are also of fundamental importance for both the structure and function.

For the above reasons, several studies have been carried out on the structure and dynamics, and on lipid–protein interactions of membranes, employing a wide variety of different physical techniques. Such techniques are, for instance, nuclear magnetic resonance (NMR), electron spin resonance (ESR), Fourier transform infrared (FTIR), and Raman spectroscopies, fluorescence techniques, X-ray crystallography and diffraction, electron microscopy, differential scanning calorimetry (DSC), and circular dichroism. The com-

plexity of biological systems often requires the combined use of several techniques, which might result in a better insight into the nature of the object studied.

Although much valuable information has been derived from such studies [9–15], many details of membrane properties, protein structure and function, and lipid–protein interactions are still to be explored.

In this thesis, an attempt has been made to synthesize two of the above mentioned experimental approaches, ESR and FTIR spectroscopy, to get a deeper insight into the organization, structure and dynamics of higher plant thylakoid membranes. These membranes are the primary places of the solar energy conversion, thus being the source of any form of life on Earth. Therefore, understanding their functioning is one of the fundamental problems of science. Even small steps in this process can be rewarding and challenging.

Chapter 2

Literature

Both Fourier transform infrared and electron spin resonance spectroscopy have proved to be valuable tools in the analysis of biological membranes. These techniques complement each other because FTIR spectroscopy detects molecular vibrations on a very short time scale (10^{-14} s) providing a "molecular snapshot" of the molecules under investigation, whereas ESR spectroscopy has a time window (10^{-7}–10^{-11} s) that covers acyl rotational isomerization, and the rotational and translational diffusion of lipids.

In this chapter, a brief description of how they can be applied to study lipid order, protein structure, membrane dynamics, and lipid–protein interactions will be presented. In the last section, open questions concerning thylakoid membrane structure will be discussed, those questions we are going to deal with in this thesis.

2.1 Fourier transform infrared spectroscopy

Infrared (IR) spectroscopy is based on the absorption of electromagnetic radiation by matter due to different vibrational modes of the chemical bonds present in the various groups of a molecule.

The invention of the fast Fourier transform algorithm [16] has permitted the development of a new generation of infrared instruments based on the long-existing Michelson interferometer [17, 18] and resulted in a renewed interest in the use of IR spectroscopy for studying biomolecules. Besides its high wavenumber accuracy, FTIR allows much higher signal-to-noise ratios and much higher resolving power as compared to dispersive instruments [18–21].

FTIR spectroscopy has a number of favourable features for the study of biological systems: spectroscopic probes which may perturb the behaviour of the molecules are not required; samples may be studied in a variety of physical states (solids, solutions, dispersions, oriented films); only small amounts of material are normally required; spectra

can be measured very quickly (in fractions of a second); studies of intact membranes and living cells as well as model membrane systems are possible; it provides structural and dynamics information from both acyl chain and headgroup of the lipid molecules, and also provides information about the structure and dynamics of the protein components simultaneously in a single experiment.

2.1.1 FTIR study of lipids

The polymorphic phase behaviour, the conformation and dynamics of lipids have great relevance to membrane function [2, 22–24]. FTIR spectroscopy on vesicles, monolayers, bilayers, or multibilayers as well as on native membranes has been successfully used to examine many structural properties of lipids, such as their conformation, orientational order, phase transitions, phase separation in multicomponent systems, state of ionization, ion binding, hydration, hydrogen bonding and others.

Lipids absorb in many different regions of the IR spectrum [25, 26]. Spectral features can originate from molecular vibrations of the various functional groups in the headgroup, and from those of the acyl or alkyl chains. Approximate frequencies of some important vibrational modes are listed in Table 2.1.

Table 2.1: Some important infrared absorption bands of membrane lipids

Assignment	Approximate frequency (cm^{-1})
olefinic =CH stretch	3010
CH_3 antisymmetric stretch	2956
CH_2 antisymmetric stretch	2920
CH_3 symmetric stretch	2870
CH_2 symmetric stretch	2850
ester C=O stretch	1730
$N^+(CH_3)_3$ antisymmetric bend	1485
CH_2 scissoring	1470
CH_3 antisymmetric bend	1460
$N^+(CH_3)_3$ symmetric bend	1405
CH_3 symmetric bend	1378
CH_2 wagging band progression	1200–1400
PO_2 antisymmetric stretch	1228
PO_2 symmetric stretch	1085
CH_2 rocking	720–730

The CH stretching vibrations give rise to bands in the spectral region 2800–3100 cm^{-1}. The CH_2 antisymmetric stretching mode ($\nu_{as}CH_2$) at around 2920 cm^{-1} and the CH_2 symmetric stretching mode ($\nu_{sym}CH_2$) at around 2850 cm^{-1} are generally the strongest

bands in the spectra of lipids. The frequencies of these bands are conformation-sensitive and respond to changes in the ratio of *gauche* and *trans* conformers along the lipid acyl chains [25, 26]. The other bands in this region can be assigned to the vibrational modes of the terminal CH_3 groups at 2956 cm^{-1} (antisymmetric stretch) and 2870 cm^{-1} (symmetric stretch), and of the =CH stretching band (at 3010 cm^{-1}) of the unsaturated acyl chains. The methylene stretching vibrations are particularly useful in characterizing the gel to liquid-crystalline phase transition and acyl chain conformations of lipids [25, 26]. In practice, in most cases $\nu_{sym}CH_2$ band is monitored because it is freer from overlap by other vibrational modes. Its frequency has been shown to increase by 2–5 cm^{-1} at the gel to liquid-crystalline phase transition temperature. As illustrated in Fig. 2.1, the frequency of the CH_2 symmetric stretching band increases from about 2851 cm^{-1} in the gel state to about 2854 cm^{-1} in the liquid-crystalline state of dipalmitoylphosphatidylcholine (DPPC) at the transition temperature (T_m) ≈41 °C, due to the increase in the *gauche/trans* conformer ratio in the acyl chains. The width of the band also increases due to the increased motional rates and to the larger number of conformational states of the hydrocarbon chains in the liquid-crystalline state. Numerous naturally occurring

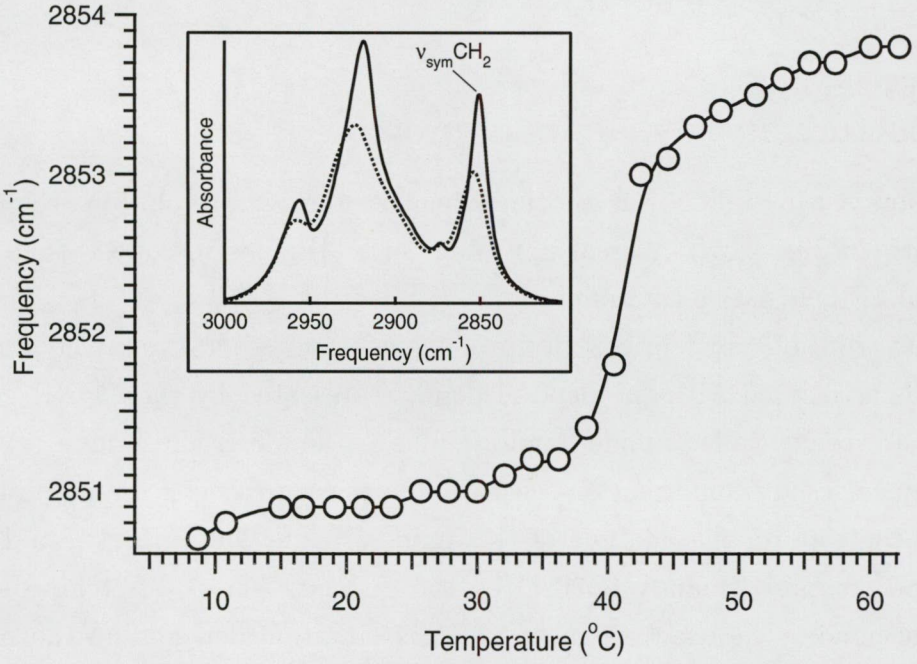

Figure 2.1: Frequency shift of the $\nu_{sym}CH_2$ band of the FTIR spectrum of DPPC. The inset shows the CH stretching region of DPPC spectra at 8 (solid line) and 62 °C (dotted line).

lipids are known to exhibit non-lamellar phases [23, 27, 28]. The bilayer to non-bilayer phase transition was characterized by FTIR spectroscopy in phosphatidylethanolamines as described in [29].

There are other vibrational modes of the methylene and methyl groups in the region of 700–1500 cm^{-1} (Table 2.1). The CH_2 scissoring mode, for example, gives rise to bands around 1470 cm^{-1}; the number of these bands and their exact frequency are dependent on acyl chain packing and conformation [30]. Spectral parameters of methylene scissoring, rocking, and wagging modes, as well as of CH stretching modes can be used to monitor the packing of acyl chains and thus to determine the nature of pretransition events [31].

Vibrational modes of the moieties found in the headgroup of membrane lipids also give rise to a number of infrared bands. The most useful ones for probing the interfacial region of lipids are the ester group vibrations. The C=O stretching bands in the region of 1700–1750 cm^{-1} are the most intense of the headgroup bands. The position of these bands is sensitive to the hydrogen bonding, to the geometry of the glycerol moiety and the packing of the acyl chains [32]. In diacyl lipids, this region consists of at least two bands found at 1725 and 1742 cm^{-1}. In general, in hydrated samples, only a broad band contour is found, however, resolution enhancement techniques usually reveal two or more of the constituent bands [25, 30].

Several studies have demonstrated that FTIR spectroscopy is a powerful method for obtaining molecular conformational information not only from model membranes but from live cells as well [11, 33].

2.1.2 Structure and dynamics of proteins

IR spectroscopy is a useful tool as a complement to the high-resolution techniques in protein studies [20, 30, 34–37]. A great advantage of FTIR spectroscopy is that proteins can be studied in their native environments.

The IR spectrum of polypeptides and proteins contains several relatively strong absorption bands associated with the peptide bond, represented by the CONH grouping. These bands are the so-called amide bands (amide A, amide B and amide I–VII) [20]. All amide frequencies are conformation-sensitive, but most works concerning protein conformation concentrate on the analysis of the amide I band, located between 1600 and 1700 cm^{-1} and composed mainly ($\approx$80%) by the carbonyl (C=O) stretching vibration of the peptide bond. The exact frequency of this vibration depends on the nature of hydrogen bonding involving the C=O and NH moieties; this in turn, is determined by the particular secondary structure adopted by the polypeptide chains.

Most biological systems require water for proper functioning. Therefore, investigations on structure and function is mostly performed in the presence of water. Since the H_2O bending mode at around 1643 cm^{-1} overlaps with the amide I band, the subtraction of the water spectrum must be accomplished before studying the protein spectrum. Alternatively, D_2O is often used instead of H_2O during sample preparation because due to the

isotope effect, the bands of D_2O are downshifted leaving the amide I region free [20, 30]. It should be noted here that the use of D_2O causes 0–10 cm^{-1} and about 100 cm^{-1} bandshifts in the amide I and II regions, respectively (see H–D exchange on page 8). Therefore, bandshapes in H_2O and D_2O can differ due to the shift of components [20], but the structure does not necessarily have to be affected, and maintenance of the biological activity does in fact support the idea that protein conformation is still preserved. Moreover, the isotopic shift can help in discriminating between bands that are very difficult to resolve.

Some typical frequency ranges with the corresponding secondary structures are shown in Table 2.2. It should be stressed that these correlations are guidelines only, and while

Table 2.2: Correlations between common protein structures and amide I frequency in D_2O

Structure	Amide I frequency (cm^{-1})
Antiparallel β-sheet/aggregated strands	1675–1695
Turns	1660–1685
3_{10}-helix	1660–1670
α-helix	1648–1660
Unordered	1640–1648
β-sheet	1625–1640
Aggregated strands	1610–1628

they will prove to be adequate for IR spectroscopic studies on most proteins and peptides, there are proteins and peptides that contain secondary structures that absorb outside the frequency range given in the table [30, 38]. Therefore, a critical step in the interpretation of IR spectra of proteins is the assignment of the amide I component bands to different types of secondary structure.

The observed amide I band contours of proteins are usually complex composites that consist of a number of overlapping component bands, representing helices, β-sheets, turns and unordered structures. Information on protein secondary structure can be obtained by comparing the infrared spectrum of an unknown protein with a set of spectra (calibration set) from proteins with known structure [39, 40], or else by decomposing the amide I band into constituents by curve fitting [41–43]. Several approaches have been developed that allow visualisation of overlapping bands following manipulation of the spectrum. They can be used to estimate the number of components for an iterative least-squares curve fitting analysis from which one can obtain quantitative information on the secondary structure composition of the protein. A very effective procedure is Fourier self-deconvolution which achieves band narrowing in the spectrum at the expense of the signal-to-noise ratio [44–47]. Increased separation of the overlapping bands can also be achieved by calculating higher

derivatives of the absorption spectrum, either in the frequency domain [48] or through mathematical manipulations in the Fourier domain [49]. A distinct advantage of the Fourier deconvolution method is that it introduces less distortion to the spectra. In particular, it does not affect the integrated intensities of the individual component bands. Despite their apparent simplicity, these procedures present a number of experimental problems which are not fully appreciated by some investigators and thus lead to artifacts, therefore, they must be used with great care [50,51]. Two important factors are the signal-to-noise ratio of the spectrum and the water vapour which gives rise to narrow absorption bands in the region overlapping the amide I mode.

FTIR spectroscopy is also useful for investigating hydrogen–deuterium exchange of the peptide groups in proteins and polypeptides. The most significant change in the spectra of a protein in D_2O compared with that in H_2O is the marked reduction in intensity that occurs with the amide II band. This is a reflection of isotopic substitution of the peptide bond N–H to N–D, which shifts the amide II band to lower frequency by about 100 cm^{-1}. The hydrogen–deuterium exchange rate is extremely sensitive to the local environment of the peptide group and to the overall conformational dynamics of the protein and can therefore be used to monitor perturbations in protein conformation that may be brought about by different factors, such as ligand binding, pH and temperature. Thus, examining the amide I and amide II bands may be very informative on structural changes, thermal stability and protein dynamics [52–55].

Amino acid side chains play fundamental roles in stabilising protein structures and in catalysing enzymatic reactions. Their absorption provides very valuable information when the mechanism of protein reactions is investigated. For a review on this field see [56].

As the great number of publications demonstrates, FTIR spectroscopy has become an established tool for the structural characterization of proteins. However, correct results can only be obtained if the investigator has a full understanding of the strengths and limitations of the method used [30,50,51].

2.1.3 Lipid–protein interactions

Studies of lipid–protein interactions are obviously of central importance in understanding biological membrane structure and function. Although such studies have been made using a wide variety of physical techniques (e.g. DSC [57], ESR [58] and NMR [59] spectroscopy) providing much valuable information, our understanding of the details of lipid–protein interactions remains incomplete. This is due in part to the complexity of natural membranes.

As mentioned above, FTIR spectroscopy is a suitable technique to study lipids and proteins simultaneously in different environments. Accordingly, it has been also used

to study lipid–protein interactions. Information on both the effect of proteins on lipid conformation and phase behaviour, and the effect of lipids on protein structure can be obtained in model, as well as in natural biomembranes [7, 30]. To obtain information on conformational order of lipids, monitoring the frequency of the CH_2 symmetric stretching band has been demonstrated as a very useful tool in complex membranes as well. On the other hand, amide I region is free from lipid vibrations, that assures the simultaneous possibility of structural investigation of proteins.

In the presence of proteins, because of the decrease in phase cooperativity, usually there are no such clear, sharp phase transitions as compared to the pure lipid systems, the transition shows considerable broadening [7, 60] and sometimes also shift in the transition temperature [7, 61]. Furthermore, biological membranes are generally in the fluid liquid-crystalline phase which is needed to ensure optimal membrane function, therefore phase transitions may be absent completely in the physiological temperature range. The $\nu_{sym}CH_2$ frequency, which is a measure of the *gauche/trans* ratio of the acyl chains, can be influenced not only by temperature but also by the nature of the protein interacting with lipids and the lipid/protein ratio [43]. Proteins contacting their lipid environment can either increase or decrease the content of *gauche* conformers [7, 60, 61]. Moreover, their influence may differ or may be opposite in the gel and liquid-crystalline phases or at different temperature ranges.

An example how lipids can affect on the structure and thermal stability of proteins is the destabilization of an extrinsic membrane protein, cytochrome c, upon binding to the surface of certain model membranes [62]. It has been demonstrated that binding of ferricytochrome c to model membranes containing an acidic phospholipid, phosphatidylglycerol, results in an overall destabilization of the protein structure. It is indicated by an increased accessibility of the backbone amide groups to hydrogen–deuterium exchange (resulting in a shift to lower wavenumbers of the protein amide I vibrational mode), and by the decreased thermal stability of the membrane-bound protein, as evidenced from the temperature dependence of IR spectra and from direct thermodynamic measurements using DSC. A similar study can be found in [63].

2.1.4 Isotopes as specific labels

The complexity of natural membranes, and studies involving the addition of other substances to lipid bilayers often precludes the observation of specific bands. In such a situation, labelling specific parts of a molecule (lipid or protein) allows us to monitor them directly. The use of lipids with fully or partially deuterated acyl chains provides a good example. The C–D stretching frequencies, which are approximately the C–H frequencies divided by $\sqrt{2}$, occur between 2000 and 2300 cm^{-1}, a spectral region generally

free of interfering absorption bands. Similarly to the frequencies of C–H stretching bands, the frequencies of the C–D stretching bands are also sensitive to the conformation and to the *gauche/trans* ratio in the deuterated acyl chain segments. Acyl chain perdeuterated dimyristoylphosphatidylcholin and dimyristoylphosphatidylserine were incorporated into human erythrocytes, and the asymmetric CD_2 stretching frequency was measured by Moore *et al.* [11]. These experiments demonstrated that FTIR spectroscopy can be utilized to monitor directly a specific species from the entire phospholipid population. Specifically deuterated derivatives of DPPC were used by Mendelsohn *et al.* to determine the conformational disorder in the acyl chains at particular depths in the bilayer by monitoring the CD_2 rocking modes [64]. Labelling of proteins is also possible. The application of ^{13}C labelling shows the potential of studying protein–protein interactions using FTIR spectroscopy [65].

2.2 Electron spin resonance spectroscopy

Electron spin resonance (or electron paramagnetic resonance) spectroscopy is a sensitive tool for the detection of paramagnetic species (e.g. free radicals, transition metal ions). It is based on the detection of the resonance absorption between the Zeeman levels of a paramagnetic system situated in a static magnetic field. Except for short-lived free radicals and fast-relaxing metalloproteins, biomembranes are transparent to ESR spectroscopy unless stable free radicals are introduced (spin-labelling) [66].

Spin-label ESR spectroscopy has become a very useful technique for examining biological membranes, because it has an optimal time scale to study membrane dynamics [67]. Membrane spin-labelling means either the intercalation of a stable nitroxide free radical, usually nitroxyl analogues of natural lipids or fatty acids, into the membrane or covalent modification of membrane protein amino acid side chains [68]. The ESR spectra of these probes, which comprise three hyperfine lines resulting from the coupling of the unpaired electron spin with the nitrogen nuclear spin, are sensitive – among other factors – to molecular motions, and also to the nature of the medium in which the probe is dissolved [66]. Thus, information can be obtained regarding the physical state and dynamic properties of the membrane and membrane constituents (e.g. mobility, lipid order, polarity) [69–71].

Most of the commercial ESR spectrometers work in the X-band (9 GHz) region. Experiments carried out at higher frequencies (Q-band: 34 GHz, W-band: 94 GHz) provides an enhanced sensitivity to both fast and slow motional regimes. Thus, high field measurements can be very useful for separating components which strongly overlap in the X-band spectra [72, 73].

The available computational power today allows making powerful ESR line-shape cal-

culation programs. These simulation programs can not only be used for a better understanding of the nature of ESR spectra, but often also for the direct analysis of experimental data [74,75].

2.2.1 ESR and membrane dynamics

The time window of conventional ESR spectroscopy is determined by the spectral anisotropy of the nitroxide group of the spin-label and ranges between 10^{-11}–10^{-7} s, which optimally matches the time scale of the rotational motions of the lipids in membranes. When the molecular reorientational motion of the nitroxyl group is slow, the spectrum of randomly oriented molecules consists of a set of overlapping spectral lines corresponding to different orientations. As the tumbling rate increases, the anisotropic lineshape transforms to a single, motionally averaged isotropic spectrum with narrower lines. A simple equation utilizing the line widths (or line heights) of the spectra can be used to obtain an approximate value of the rotational correlation time (τ_R) [76]. If τ_R cannot be evaluated the height of the central line can be monitored, which changes steeply at phase transitions. An other frequently used parameter, which is a measure of the orientational order (i.e. mobility) of the lipid acyl chain segment bearing the nitroxyl, is the order parameter. It can be defined as

$$S = (\overline{A}_{\parallel} - \overline{A}_{\perp})/(A_{zz} - \frac{1}{2}(A_{xx} + A_{yy})) \tag{2.1}$$

where $\overline{A}_{\parallel}$ and $\overline{A}_{\perp}$ are the motion-averaged hyperfine splittings measured from the experimental spectra, and A_{xx}, A_{yy} and A_{zz} are the principal values of the hyperfine tensors measured in the absence of molecular motion and in an environment of similar polarity [66]. In practice, the splittings between the spectroscopic peaks and troughs (see the outer ($2A_{max}$) and inner ($2A_{min}$) splittings in Fig. 2.2) and the values obtained from single-crystal measurements for A_{xx}, A_{yy} and A_{zz} are used to calculate the order parameter, and an approximate order parameter (S^{app}) is obtained. Since A_{min} is only approximately equal to $\overline{A}_{\perp}$, and the polarity of the environment of the experimental sample may differ from that corresponding to the single-crystal measurement, to calculate S using S^{app}, a correction for A_{min} and for the polarity is needed as described in [77]. A common method is simply to report $2A_{max}$, the distance between the outermost ESR lines (outer splitting), when this quantity is measurable [78]. Both S and τ_R are widely used parameters for detecting changes in membrane dynamics induced by different factors [79–81]. In addition, using lipids that are labelled at different carbon atoms along the hydrocarbon chain it is possible to study the molecular mobility at various depths in the membrane [82,83].

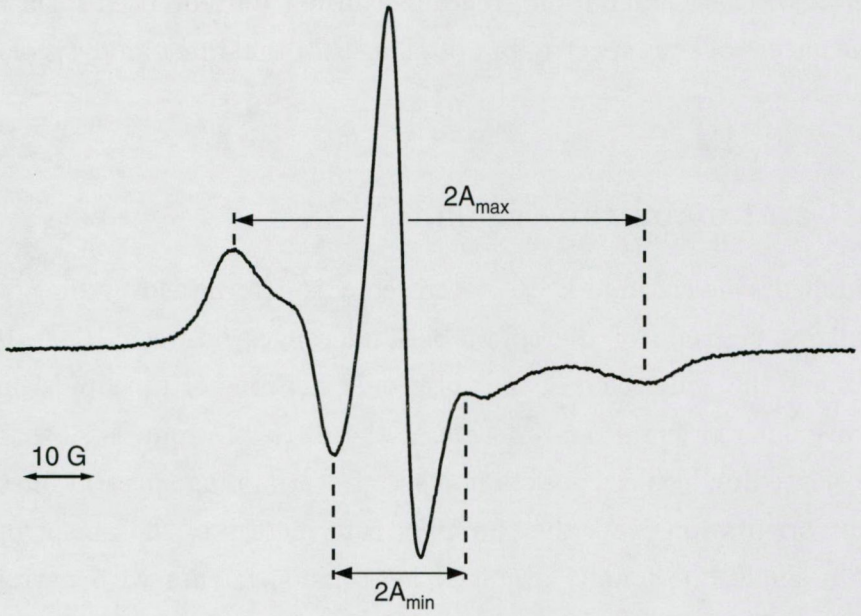

Figure 2.2: A typical ESR spectrum of a spin-labelled membrane. Spectral parameters $2A_{max}$ and $2A_{min}$ are indicated.

A different approach to obtain information about membrane organization (e.g. lipid order, rates of motion of small organic molecules in the membrane phase) is based on the partitioning of a rapidly tumbling small spin-label between the lipid and aqueous phases. The partition coefficient depends on how densely the lipids are packed. In both environments, the spectrum consists of three sharp lines. The spectral parameters, the hyperfine tensor and the g-value are slightly different in the two phases, which results in a composite spectrum where the two components are at least partially resolved. Thus, lipid phase transitions can be monitored by taking the ratio of the peak heights of the resolved (high-field) line (see Fig. 5.6 on page 28) [84].

Since the above mentioned spectral parameters are sensitive to the motional freedom of the membrane molecules, they are particularly useful for characterizing phase transitions, fluidity and lipid order [69, 71, 85].

Several biochemical processes involve lateral movement of the components within the bilayer. Due to spin–spin interactions, the ESR spectrum is sensitive to the collision frequency of the spin-label molecules incorporated into membranes, which depends on their concentration and lateral diffusion. A method for measuring lipid lateral diffusion coefficients is shown in [86].

2.2.2 Lipid–protein interactions as seen by ESR

Besides that the methods in Section 2.2.1 generally can also be used for studying complex biological membranes, the sensitivity of spin-label ESR spectroscopy to membrane dynamics has a valuable consequence. In natural membranes or in lipid–protein complexes, two-component ESR spectra are usually obtained indicating the presence of two lipid populations with different mobilities [67]. The lipids at the interface of the proteins are immobilized and thus the corresponding bulk and protein-associated components are very well resolved in the ESR spectrum of spin-labelled lipids. The fraction of the two components can be readily determined either by spectral subtraction or by spectral addition of the two components. Alternatively, spectrum simulation can also be applied. It is then possible to quantitate both the stoichiometry and the selectivity of the interactions of different spin-labelled lipids with the protein, and to study the dynamics of the protein-associated lipids [58,67,87]. A representative composite ESR spectrum is shown in Fig. 2.3. Determining the relative amount of motionally restricted (i.e. protein-interacting) spin-

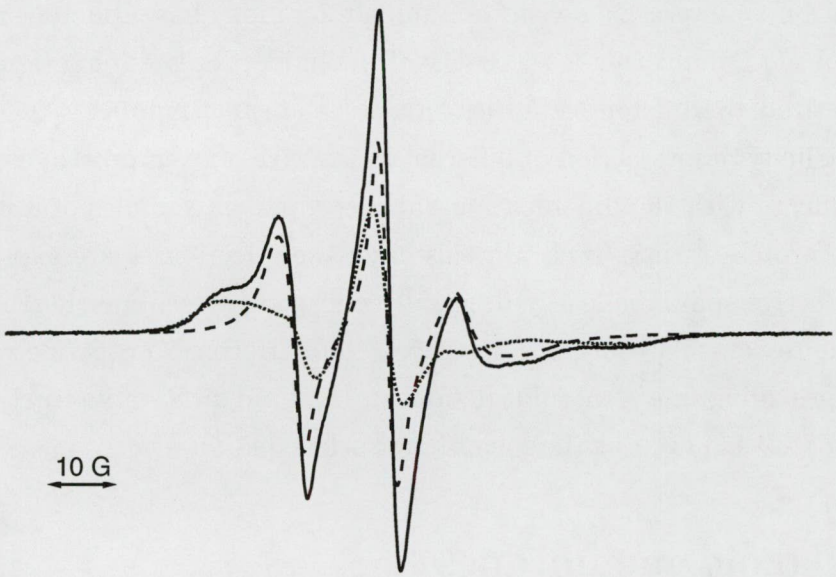

Figure 2.3: A representative two-component ESR spectrum. The mobile (dashed line) and immobile (dotted line) components are also indicated.

labelled lipids as a function of lipid/protein ratio (lipid/protein titration), the number of lipid association sites of the protein (N_b) and the relative lipid association constant (K_r) can be obtained according to Eq. 2.2:

$$(1 - f)/f = (n_t/N_b - 1)/K_r \tag{2.2}$$

where f is the experimentally obtained fraction of spin-labelled lipid associated with the protein, and n_t is the total lipid/protein ratio [58]. In case of exchange equilibrium of a spin-labelled lipid (L^*) interacting with a protein (P) in a background of unlabelled lipid (L), such as

$$L_{N_b}P + L^* \rightleftharpoons L_{N_b-1}L^*P + L\,,$$

K_r can be defined by:

$$K_r = \frac{[L^*P]\,[L]}{[LP]\,[L^*]}. \tag{2.3}$$

Such lipid/protein titration experiments yield rather detailed insight into the stoichiometry and specificity of lipid association with the hydrophobic interface of integral membrane proteins [58,88]. The number of motionally restricted lipids per protein can be determined also without applying the lipid/protein titration method above, using a non-selective spin-labelled phospholipid, for which $K_r \approx 1$. Different spin-labelled lipids (e.g. possessing different headgroups) interacting with the same protein may have different motionally restricted fractions (f), indicating a selectivity of the lipid–protein interaction that is found to be characterized by different affinities, K_r, for the same number, N_b, of association sites. The specificity of interaction of different lipids with a given protein can be obtained from measurements with the different spin-labelled lipids in samples of a fixed composition and lipid/protein ratio as well. In this case, the selectivities are expressed relative to the least selective spin-labelled lipid, usually phosphatidylcholine. Further details can be found in the review [58]. Such studies have been performed for a wide range of membranes, often providing fine structural details on the lipid–protein interactions and their dynamics [53,85,89–93] even at the membrane surface [94,95].

2.3 Thylakoid membranes

Photosynthesis in higher plants, algae and cyanobacteria takes place in the thylakoid membranes. These membranes of chloroplasts and cyanobacteria, delicate assemblies of proteins, pigments and lipids, are able to transform the physical energy of light into chemical energy, and hence to organic compounds.

Angiosperm seedlings kept in light, develop well-functioning chloroplasts with an advanced inner thylakoid membrane system housing the photosynthetic machinery. The plastids of dark-grown seedlings differ significantly. Proplastids develop into etioplasts which have a three-dimensional semicrystalline array of internal membranes, the prolamellar body, and contains the chlorophyll (Chl) precursor protochlorophyllide instead

of chlorophyll and remarkably high amount of monogalactosyl diacylglycerol (MGDG). Upon illumination, etioplasts are transformed into chloroplasts (greening), which involves the synthesis of chlorophylls and many polypeptides, and a large reorganization of plastid structure [96, 97]. Protochlorophyllides are rapidly converted to Chl which is parallelled with the disorganization of the prolamellar bodies and formation of planar thylakoid membranes (primary lamellae). Since the subsequent synthesis, assembly and modification of pigment, lipid and protein components may last for days until mature thylakoids appear [98], this process is a very useful model to study the light-controlled development of the thylakoid membrane. Although a number of studies have been carried out on the differentiation of thylakoids [99–104], our knowledge about the physical background of structural changes is still far not complete.

Besides the specific proteins and the pigments, the lipid composition of the thylakoid membranes is also uniquely specific. In thylakoid membranes of green plants, MGDG accounts for around 50% of the total lipid content. MGDG and certain other lipids were shown to be involved in strong and specific lipid–protein interactions [105, 106].

The importance of phosphatidylglycerol (PG) – which accounts for 5–12% of the total lipid content – in the organization and functioning of thylakoid membranes also has been demonstrated in several studies [107–109]. The phase transition of membrane lipids and the chilling sensitivity of plants were long ago postulated to be related. It was thought that the membrane lipids of chilling-sensitive plants enter the gel phase at chilling temperatures, whereas those of chilling-tolerant plants remain in the liquid-crystalline phase. In higher plant thylakoids, however, phase transition of membrane lipids has not been seen. A correlation between the chilling sensitivity and the extent of unsaturation of the fatty acids of thylakoid membrane lipids was found only when the individual lipid classes were analysed. In the chloroplast membranes of herbaceous plants, there was a clear correlation between the chilling sensitivity and the level of saturated and trans-monounsaturated molecular species (known as 'high-melting-point' molecular species) of PG [110, 111]. A similar correlation has been observed for a wide variety of higher plants [111, 112]. These molecular species undergo the gel to liquid-crystalline phase transition at around room temperature, as demonstrated on isolated PG molecules in a model system [113]. *In situ*, however, the phase transition of thylakoid membranes has not been detected in the physiological temperature range. This failure might have been due to the low amount of high-melting-point PG in the thylakoid membrane and by the imperfect sensitivity of the methods applied.

Chapter 3

Aims

In this work, mainly two complementary spectroscopic techniques, Fourier transform infrared and electron spin resonance spectroscopy, were used to study membrane structure and dynamics, and lipid–protein interactions in different model and photosynthetic membranes. The aims of these studies were as follows:

1. development and validation of new methods to enhance the performance of FTIR and ESR spectroscopic techniques via

    - improved spectrum analyses studying the CH_2 stretching vibrations of lipids and ESR spectra of TEMPO spin-label
    - combination of complementary spectroscopic data,

2. to gain more insight into the molecular details of structural rearrangements in developing thylakoid membranes during greening,

3. to obtain information on the structural role of PG in genetically manipulated tobacco thylakoids with different character of chilling sensitivity.

Chapter 4

Materials and Methods

4.1 Chemicals and materials

Chemicals

1,2-Dioleoyl-*sn*-glycero-3-phosphocholine (DOPC), 1,2-dipalmitoyl-*sn*-glycero-3-phosphocholine (DPPC), D_2O, and the spin-labels 5-(4',4'-dimethyloxazolidine-*N*-oxyl)stearic acid (5-SASL) and 2,2,6,6,-tetramethylpiperidine-1-oxyl (TEMPO) were purchased from Sigma.

Plant materials

Barley. Barley (*Hordeum vulgare* L. cv. Triangel) was grown from seed in vermiculate in complete darkness at 25 °C. After 6 days of growth under normal condition, except for the darkness, seedlings were illuminated continuously with 100 μmol·m^{-2}·s^{-1} white light. Samples were taken at 0, 6, 12, 24 and 48 h of illumination and only the middle part of the leaves, obtained by cutting off 0.5 cm segments from both ends of leaves, were used for analyses. Plastids were isolated at ≈0 °C in a medium containing 0.4 M sorbitol, 10 mM NaCl, 5 mM $MgCl_2$, 1 mM $MnCl_2$, 1mM phenylmethanesulfonyl fluoride (PMSF) and 50 mM 2-morpholinoethanesulfonic acid monohydrate (MES) (pH 6.5). The isolated plastids were disrupted by osmotic shock in a medium containing 40 mM sucrose, 10 mM NaCl, 5 mM $MgCl_2$, 1mM PMSF and 20 mM tricine-KOH buffer (pH 7.8). The thylakoid membranes were stored at –80 °C.

Tobacco. Transgenic tobacco plants (*Nicotiana tabacum* var. Samsun) were obtained as described in [114]. All plants were grown according to Moon *et al.* [115]. Thylakoid membranes were prepared according to Leegood and Malkin [116], with the modification that the thylakoid membranes obtained with their method were further purified on a step-wise gradient made with 21%, 27%, 45% and 60% Percoll (Pharmacia, Uppsala, Sweden) in a 50 mM tris(hydroxymethyl)aminomethane hydrochloride (Tris-HCl) buffer (pH 7.8)

containing 0.3 M sucrose, 20 mM NaCl, and 5 mM $MgCl_2$. The gradient was centrifuged at 13,000 g for 30 min. After centrifugation, the thylakoid membranes were collected from the Percoll gradient, resuspended in the same buffer, and collected by centrifugation. The thylakoid membranes were stored at –80 °C.

4.2 Sample preparation

FTIR measurements

Homogeneous catalytic deuteration of the unsaturated fatty acyl chains of DOPC vesicles was carried out as described in [117,118]. As a result, the Δ^9 double bond of the oleoyl chain was saturated and the C_9 and C_{10} carbon atoms became labelled with deuterium atoms. The catalytic reaction was stopped after different time intervals to obtain different levels of saturation. After deuteration, lipids [mixtures of dioleoyl- (DOPC), 1-oleoyl-2-stearoyl- (OSPC) or 1-stearoyl-2-oleoyl (SOPC), and distearoyl-phosphatidylcholines (DSPC)] were extracted from the liposomes and dissolved in chloroform. This chloroform solution was deposited on the surface of a CaF_2 window, dried under vacuum and hydrated with D_2O.

DPPC samples were prepared in the same way as that of the lipid mixtures above.

50 μl aliquots of barley thylakoid membrane suspension (corresponding to 600–750 μg protein) were pelleted (12,500 g, 10 min) and resuspended in 500 μl buffer, which was the same as for membrane preparation but D_2O-based, and centrifuged again. The pellet was placed between CaF_2 windows using a spacer of 20 or 25 μm. The edges of the windows were sealed with silicon grease to avoid water evaporation during temperature scans.

In the case of tobacco thylakoid, 100 μl aliquots of thylakoid membrane suspensions were diluted with 1 ml D_2O-based 10 mM 4-(2-hydroxyethyl)piperazine-1-ethanesulfonic acid (HEPES) buffer, pD 7.0, centrifuged for 15 min with a Beckman TL100 centrifuge at 85,000 rpm, resuspended in 1 ml of the same buffer, and centrifuged again. Thylakoids were placed between CaF_2 windows, separated by a 25-μm-thick Teflon spacer.

ESR measurements

For spin-labelling, 5 μl of 5-SASL solution in ethanol (1mg/ml) or 10 μl of TEMPO solution in water (10 mM) was added to 100 μl barley thylakoid suspension (corresponding to 1.2–1.5 mg protein) while vortexing the sample in the dark. The sample was incubated for 10 min in the dark at room temperature and repeatedly vortexed. The spin-labelled sample was then filled into glass capillary with internal diameter of 1 mm and concentrated in a bench top centrifuge (4,000 g, 10 min). Supernatant and some pellet was removed

to obtain a sample not longer than 5 mm in the capillary. Extra care was taken to keep the length of the pellet and supernatant constant, about 2.5 mm each, in the TEMPO experiments.

4.3 Techniques

FTIR spectroscopy

Infrared spectra were recorded on a Philips PU9800 or on a Bruker IFS66 (Karlsruhe, Germany) FTIR spectrometer using DTGS or a liquid nitrogen-cooled MCT detector, at 2 cm^{-1} spectral resolution, in the interval of 900–4000 cm^{-1}; 128 or 2048 (with the MCT detector) interferograms were averaged for each sample and each background spectrum. The spectrometer was continuously purged with dry air to eliminate water vapour. The CaF_2 windows were put into a thermostated sample holder mounted on a shuttle device. The temperature of the sample holder was set by a computer-controlled water bath. The temperature-dependent measurements were performed in the 5–65 °C range by repeating the following measurement cycle: recording of the background, recording of the sample spectrum, measurement of the actual temperature on the surface of the CaF_2 window, setting of the new temperature (in 2–3 °C steps), and waiting for 7 or 10 min for the new thermal equilibrium to be established. The whole measurement cycle was computer-controlled. Data processing and spectrum analysis were carried out by using SPSERV software (Dr. Cs. Bagyinka, Institute of Biophysics, Biological Research Centre, Szeged, Hungary) and Igor Pro programming, data analysis and plotting environment (WaveMetrics, Lake Oswego, Oregon). In general, a baseline, defined in a broader spectral region than that of interest, was subtracted from the original spectra. For band-fitting analysis a set of Lorentzians were least-squares fitted either to the C–H stretching vibration region or to the 1530–1760 cm^{-1} region including lipid carbonyl and amide I–II vibration bands. In some cases singular value decomposition (SVD) was used to analyse spectral data [119].

ESR spectroscopy

The ESR spectra were recorded using an X-band Bruker (Rheinstetten, Germany) ECS 106 spectrometer equipped with a computer-controlled thermostat and a standard TE102 cavity using first harmonic in-phase detection at 100 kHz field modulation with a modulation amplitude of 1 G and 0.3 G for 5-SASL and TEMPO, respectively. Microwave power was set to 16 and 5 mW, for 5-SASL and TEMPO, respectively. Scan range was 120 G for 5-SASL and 80 G for TEMPO spectra. During one scan, 1024 points were recorded at an A/D resolution of 16 bits. Noisy spectra were recorded in accumulation

mode (2–8 scans) to improve signal-to-noise ratio. The temperature-dependent measurements were carried out from 10 to 64 °C with 3 °C steps. Five minutes were allowed to reach thermal equilibrium at the new temperatures. Data analysis was performed using the WinEPR package from Bruker, and Igor Pro. Simulation of the TEMPO spectra was made using software written as Igor procedures.

Other analytical techniques

The level of saturation after deuteration of DOPC was determined by gas chromatography of methyl esters of fatty acyl chains as described in [118].

Barley. Chlorophyll content was determined from 80% acetone extract of 0.2–0.4 g of leaf segments according to the method of Arnon [120]. Extraction and analysis of lipids of barley thylakoids were carried out as described in [121]. The total protein content of thylakoids was determined according to Markwell *et al.* [122]. Lipid fatty acid composition was determined by gas chromatography after extracting total lipids using a modified method of Folch *et al.* [123]. Sodium dodecyl sulfate polyacrylamide gel electrophoresis (SDS PAGE) was carried out as described in [124]. Chlorophyll fluorescence measurements were carried out by using a portable Hansatech Plant Efficiency Analyser in 6 receptions on 5 leaves. After 20 min dark incubation, samples were excited with the light intensity of 1600 μmol·m^{-2}·s^{-1} at 650 nm and fluorescence was detected for 60 s.

Tobacco. For analysis of tobacco thylakoid membrane lipids, lipids were extracted from the isolated thylakoid membranes according to Bligh and Dyer [125]. Classes of polar lipids were separated by ion-exchange column chromatography on silica gel, and by thin-layer chromatography on silica gel [110]. The separated lipids were esterified, and their methyl esters were analysed by gas chromatography [110].

Chapter 5

Results and Discussion

In Chapter 2, it was shown that both FTIR and ESR spectroscopy are powerful techniques for studying membrane structure and dynamics. However, there is a permanent desire to improve and refine techniques because these improvements deliver a better understanding of the system investigated. In the following sections, it will be discussed how we could make such improvements and apply FTIR and ESR spectroscopy on different model and photosynthetic membranes.

Unfortunately, space does not permit to discuss our results in every detail, thus the reader is referred also to the attached papers.

5.1 Structural rearrangements in developing thylakoids

To obtain further details about the structural rearrangements in developing thylakoids of barley, we used FTIR and ESR spectroscopy. Both the CH stretching region and the 1500–1750 cm^{-1} region, containing the amide I–II bands and lipid carbonyl vibrations, were studied and analysed in the FTIR spectra. For ESR measurements we used two spin-labels, 5-SASL and TEMPO. In every measurement, temperature was an additional parameter, which allowed to explore differences in protein stability, membrane dynamics, etc. between the membranes at different stages of greening.

5.1.1 Biochemical and functional parameters

In order to compare different experiments and sets of data, and for a better insight into structural changes of the membranes, we examined some biochemical and functional parameters as well. Here I give only a brief summary of these data; details can be found in the attached papers.

Chl accumulation defines the course of greening and serves as a reference when com-

paring different plants and experiments [124]. In our experiments, it had a lag period followed by a rapid accumulation of pigments, which slowed down after 24 h of greening.

The relative amount of 18:1 and 18:2 fatty acids did not change during greening. However, the relative amount of the three most abundant fatty acids changed significantly: the fraction of the saturated chains 16:0 and 18:0 decreased from 43% and 15% to 29% and 7%, respectively, and that of the polyunsaturated chain 18:3 increased from 15% to 42%, and their summed fraction remained between 70–78% during greening (see Table 1 in Annex V).

The SDS PAGE pattern of the thylakoid proteins changed largely upon greening, and these changes are in a good agreement with earlier reports [126]. Upon greening, bands at around 13–14 and 17–19 kDa were disappearing, while the intensity of bands at around 25–28 kDa increased about 4.3-fold. The bands disappearing upon greening were assigned earlier to two families of early light-inducible proteins (ELIPs) related to etioplast-to-chloroplast transformation [127, 128]. The most increasing band at around 25–28 kDa was earlier assigned to apoproteins of the major chlorophyll a/b light harvesting antenna complex of photosystem II (LHCII) [104, 129].

The total protein/lipid ratio was found to be ~5 mg/mg during the first 24 h and only a slight increase could be observed up to the 48th h of greening.

The rise of the photosynthetic function was characterized by the F_v/F_m ratio obtained by fluorescence induction kinetics, which exhibited the major part of its increase within the first 24 h of greening. Later the rate of the change slowed down. In agreement with the above parameters, it indicates that the functional membrane is formed after 48 h of greening.

5.1.2 FTIR spectroscopy of thylakoid membranes

In Fig. 5.1, FTIR spectra of barley thylakoid membranes and their band-fitting analysis at 6 and 64 °C for the C–H stretching and amide I–II vibration regions are given. The band at ≈2850 cm^{-1} of symmetric CH_2 vibrations was used to monitor the conformational order of lipid acyl chains. As can be seen in Fig. 5.1, this band was at higher wavenumbers (≈2854 cm^{-1}) at high temperature indicating an increased population of *gauche* conformers in lipid acyl chains. The increased width and the shape of the amide I band at 64 °C indicate a larger conformational heterogeneity of thylakoid proteins than at low temperature (Fig. 5.1). Moreover, the shoulder at around 1620 cm^{-1} suggests that large conformational changes occur with increasing temperature involving partial denaturation of proteins, since bands in this region are assigned to intermolecular β-structures [52, 130].

For the analysis of these changes and to obtain information on protein secondary structure composition and protein stability, we have chosen a strategy as follows: First, we

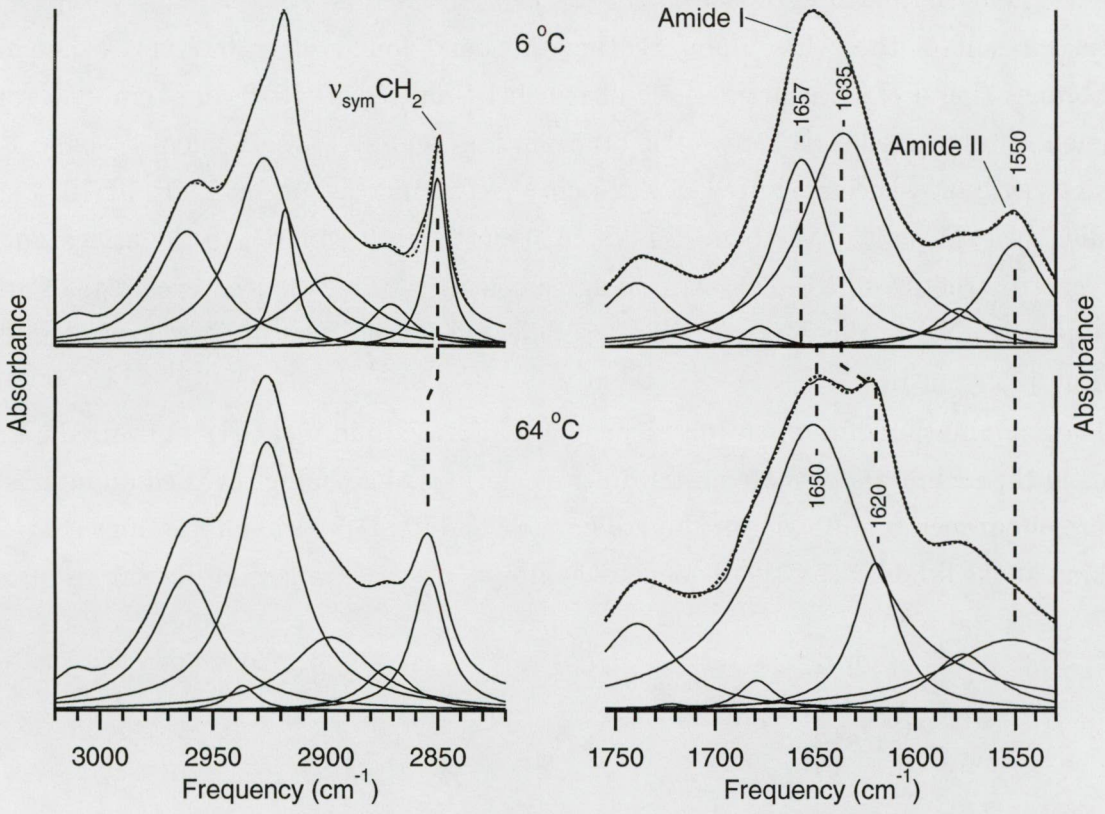

Figure 5.1: Band fitting analysis of FTIR spectra of barley thylakoid membranes in the C–H stretching (left) and in the amide I–II (right) region. The spectra were recorded at 6 (top) and 64 °C (bottom) after 48 h of greening. Experimental spectra are shown after baseline subtraction together with the Lorentzian component bands used in the fit, and their best fitting superposition (dotted line).

identified the component bands in the amide I–II region by taking the second derivative of the spectra. In the 1600–1700 cm^{-1} region, then, only the major amide I components (see Fig. 5.1 (right)) were used for band fitting allowing their parameters (intensity, position, width) free during a least-squares optimization. Keeping in mind that these components may have contributions from different type of secondary structure elements, this method was very useful to obtain a qualitative picture about secondary structure composition and stability of proteins, and to compare the membranes after different periods of greening. In the whole temperature range we obtained a good fit, which is illustrated in Fig. 5.1 (right) for 6 and 64 °C. (It should be noted here that resolution enhancement followed by a "many-components" band fitting analysis (with fixed frequency of components) gave similar results for the spectra we tested. Since this method is much more sensitive to signal-to-noise ratio, it can result in artifacts easily. Further, it was not absolutely necessary to know the secondary structure composition quantitatively since there are many different proteins in the thylakoid membrane. Therefore, we used this method only for

validating our simplified approach.)

As a result of these fits, upon heating the band found at ≈1657 cm^{-1} in mature membranes (band I/A), characteristic of α-helices, shifted to 1648–1650 cm^{-1}, a region assigned to unordered structures. The other major band at 1632–1635 cm^{-1} (band I/B), characteristic of β-sheets, shifted to 1620 cm^{-1}. The increase in intensity at 1685 cm^{-1} parallel with the shift of the band I/B to 1620 cm^{-1} can be related to the appearance of aggregated structures [51]. These are in agreement with the enhanced exchange of amide NH groups to ND in the deuterated buffer indicated by the intensity loss in the amide II band at 1550 cm^{-1}.

The examination of temperature dependence of both lipid $\nu_{sym}CH_2$ and protein amide bands in the membranes isolated after different periods of greening revealed an interesting picture about membrane structure and dynamics, and lipid–protein interactions (Fig. 5.2). Looking at the lipids, $\nu_{sym}CH_2$ frequencies exhibited a phase transition-like shift at around

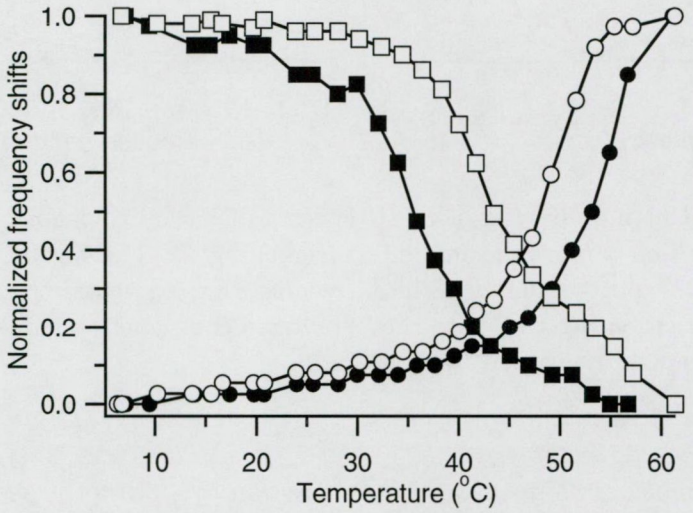

Figure 5.2: Temperature dependence of amide I/A (squares) and lipid $\nu_{sym}CH_2$ (circles) band positions after 12 h (full symbols) and 48 h (open symbols) of greening. The changes are scaled to aid comparison.

48–55 °C. This cannot be the gel to liquid-crystalline phase transition, since that is at lower temperatures. On the other hand, the amide I and amide II bands (only amide I/A is shown in Fig. 5.2) changed abruptly at ≈35–45 °C, which were followed by the upward shift of $\nu_{sym}CH_2$ frequency at ≈48–55 °C. Similar changes could be observed at any stages of greening, but the temperature at which they occurred varied during greening (see Fig. 5.2 for the 12 and 48 h data). The characteristic temperatures of the above band shifts and the middle frequencies for the two major amide I bands (obtained at 25 °C) are reported in Table 5.1 as a function of greening. The characteristic temperatures of the amide I/A and I/B components attributed to partial protein denaturing shift from 35

Table 5.1: Temperature values of steepest changes of FTIR band shifts recorded as a function of temperature and middle frequencies of selected bands at different periods of greening

	Amide I				
	T (°C)		Frequency (cm^{-1})(at 25 °C)		$\nu_{sym}CH_2$
Greening (h)	A	B	A	B	T (°C)
0	35	40	1651–1654	1624	52
6	35	40	1652–1656	1626	53
12	37	41	1654–1656	1629	55
24	41	41	1655–1656	1630	52
48	44	43	1657–1658	1632–1635	48

and 40 °C to 44 and 43 °C, respectively, with the progression of greening. Comparing the middle frequencies of these bands at 25 °C, higher wavenumbers indicate a gain in regular α-helix and β-strand structures in mature thylakoids. This is in agreement with the increased stability of the proteins. The transition temperature of the $\nu_{sym}CH_2$ frequency was the lowest (48 °C) in the fully developed membrane, which can be correlated with the increased relative amount of polyunsaturated fatty acids observed during greening.

Further aspects of the above spectral changes and comparisons with ESR data will be discussed in Section 5.1.4.

5.1.3 Spin-label ESR spectroscopy

Structures of the spin-labels used in our experiments, 5-SASL and TEMPO, are depicted in Fig. 5.3.

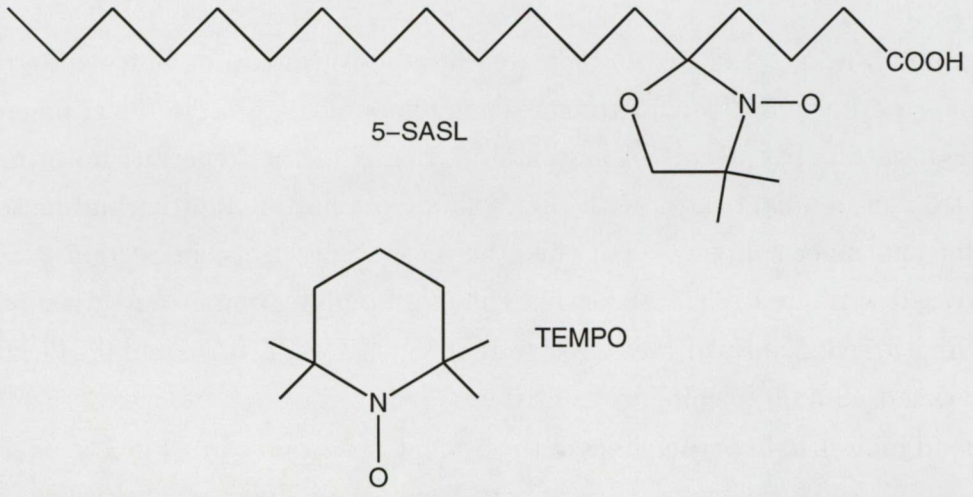

Figure 5.3: Structures of the spin-labels.

ESR spectra of 5-SASL and TEMPO in etiolated (0 h) and fully developed (48 h) thylakoid membrane dispersions are shown in Fig. 5.4. By the analysis of these spectra,

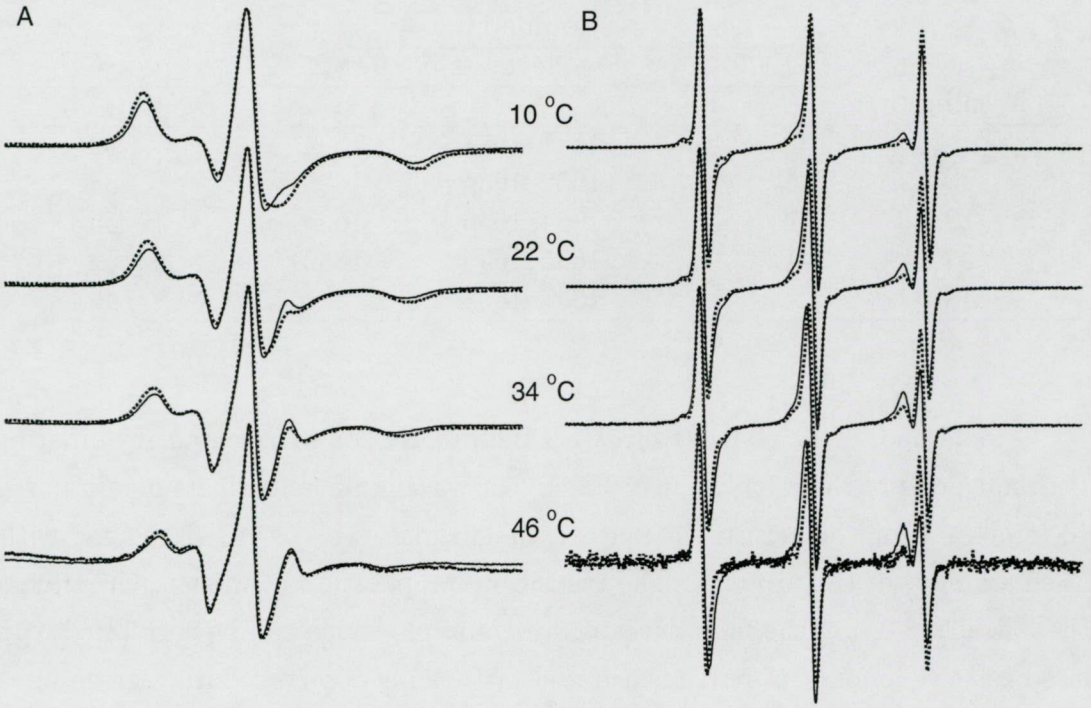

Figure 5.4: ESR spectra of 5-SASL (A) and TEMPO (B) incorporated into etiolated (dotted lines) and fully developed (solid lines) thylakoid membranes of barley. Spectra are scaled to the same amplitude.

one can show that etiolated and mature membranes differ from each other concerning lipid packing, membrane dynamics and lipid–protein interactions. For the analysis of TEMPO spectra (Fig. 5.4B), a simulation and fitting procedure was developed which is discussed in Section 5.1.3.1.

The spectra of 5-SASL (Fig. 5.4A) indicated limited rotational mobility and gradual collapse of the hyperfine anisotropy with increasing temperature both in the etiolated and fully developed states. The degree of motional averaging of the hyperfine anisotropy in 5-SASL spectra can be quantitated with the dynamic orientational order parameter (S) from the outer and inner splittings. For this, the method described in Section 2.2.1 was used. S decreased without any transition-like changes upon heating at any given periods of greening (Fig. 5.5A). Values of S at 25 °C were 0.75, 0.74, 0.77, 0.76, and 0.74 ($\pm$0.005) at 0, 6, 12, 24, and 48 h of greening, respectively.

The low- and high-field hyperfine lines of the 5-SASL spectra recorded in a temperature range of 22–40 °C were too broad to originate from single component spectra. This behaviour can only originate from a linear combination of a minimum of two (mobile and

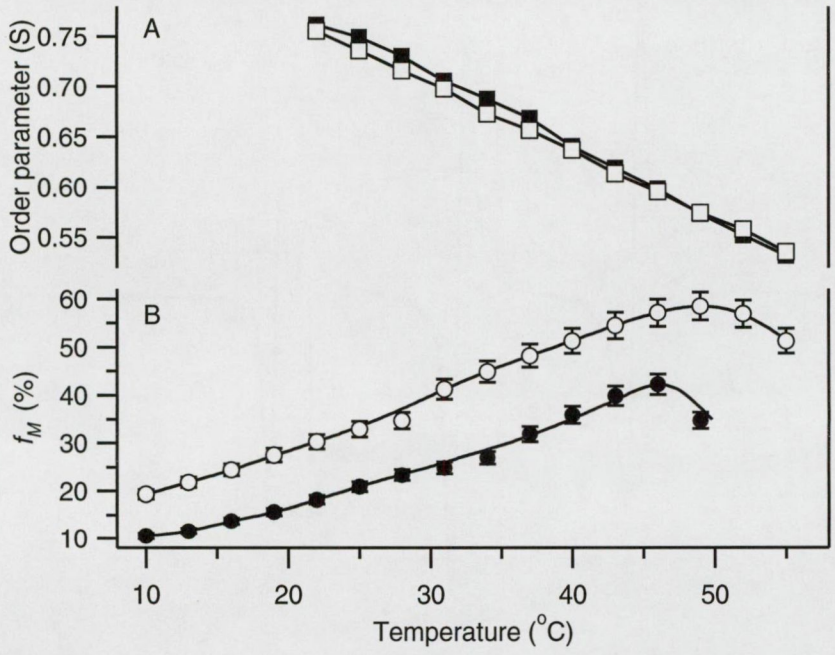

Figure 5.5: The order parameter (A), and the fraction of TEMPO spin-label partitioned into thylakoid membranes (B) as a function of temperature. (●, ■) stand for etiolated, (○, □) for mature membranes.

immobile) components with different A_{max} and A_{min} values. To determine the immobile fraction (f_i) in our spectra, an intersubtraction technique described in Section 5.1.3.2 was applied.

5.1.3.1 Development of a simulation procedure for TEMPO analysis

As mentioned in Section 2.2.1 on page 12, small nitroxide probes such as TEMPO partition between the hydrocarbon and aqueous phases of membranes. The X-band ESR spectra of TEMPO are often analysed in terms of the spectral parameter, f_t. It is an approximation of the true membrane partition parameter and can be expressed as the ratio of the least overlapping amplitudes of the split high-field line: $f_t = H/(H+P)$ where H and P, shown in Fig. 5.6, stand for the hydrophobic and polar signal amplitudes, respectively [84]. As the nitroxide line width is sensitive to motion of the probe, the temperature dependence of f_t is a combined effect of the partitioning and the changes in the rotational dynamics of the probe, and thus f_t is not a good measure of TEMPO partitioning. A 10-fold increase in g-value resolution at W-band as compared with X-band (see Section 2.2 on page 10) allows the complete resolution of the TEMPO spectrum in aqueous and hydrocarbon environments. A spectrum simulation program was developed by Smirnov *et al.* for such high field ESR spectra, which provides detailed information on the rotational motion and on the partitioning of TEMPO [72].

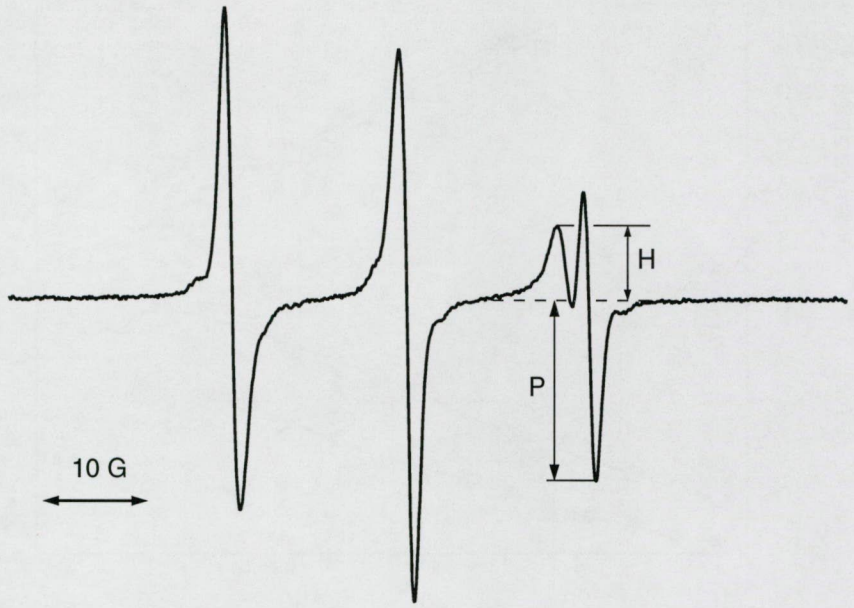

Figure 5.6: ESR spectrum of TEMPO recorded at 40 °C in thylakoid membrane. The hydrophobic (H) and polar (P) high-field signal amplitudes are indicated.

In order to analyse our X-band ESR spectra measured with TEMPO in biological membranes and to obtain more precise information on partitioning, we developed a similar spectrum simulation program and fitting procedure. The simulation program produces two triplets (i.e. membranous and aqueous ones) of derivative spectral lines with variable degrees of Lorentzian and Gaussian character (i.e. different degrees of inhomogeneous broadening) with the inclusion of ^{13}C super-hyperfine satellites and dispersion admixture to the absorption signal. (The main sources of inhomogeneous broadening are the unresolved hyperfine splitting with water hydrogens, the residual anisotropy of the g-factor and the ^{14}N hyperfine splitting, and the field inhomogeneity over the sample, while the dispersion admixture is usually caused by conductive material in the resonator). The main fitting parameters are the intensity and position of the two components, line width, hyperfine splitting constants, and ^{13}C isotope fraction in addition to a linear baseline. The value of the true membrane partition parameter, f_M, can be determined with high accuracy from the integrated intensities of the two components, I_H and I_P, of the best fitting simulated spectra obtained via the algorithm ($f_M = I_H/(I_P + I_H)$), and information can be obtained on the rotational dynamics of the spin-label.

In partitioning experiments, the spectra gradually change with the temperature, therefore, they can be processed in sequence; the best fit for one spectrum can be used as first approximation for the next one. As the hydrophobic component had a quite small intensity at low temperatures in thylakoids (see Fig. 5.7), a strategy of starting the fitting

procedure at the high-temperature end of the experimental spectra was chosen. Fig. 5.7 demonstrates the ability of the fitting procedure to extract the aqueous (C) and the hydrocarbon (B) spectra from the experimental spectrum (A).

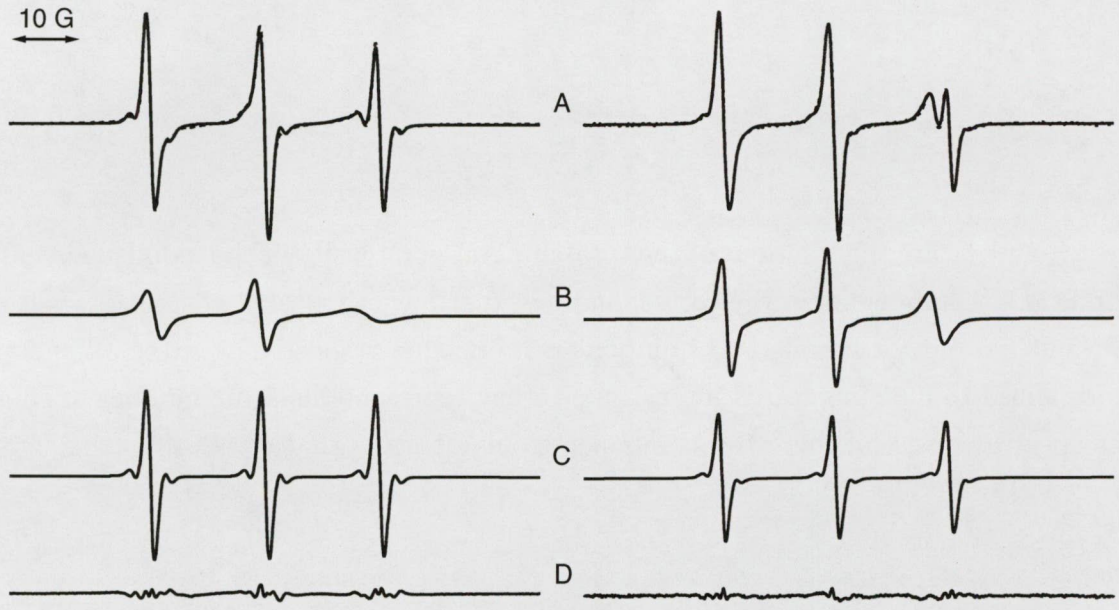

Figure 5.7: Experimental and simulated ESR spectra of TEMPO at 10 (left) and 43 °C (right). Simulated (solid line) and experimental (dashed line) spectra are essentially identical (A). (D) is the residual. The simulated spectra of TEMPO in the hydrocarbon (B) and aqueous (C) phases are also shown.

f_M, calculated from TEMPO analysis, is presented in Fig. 5.5B as a function of temperature for etiolated (0 h) and mature (48 h) thylakoids. It increased monotonically with increasing temperature until 45 °C, but dropped at ≈45–48 °C. This was true for all periods of greening. A dramatic change in f_M was also observed at different periods of greening when looked at fixed temperatures. As can be seen in Fig. 5.5B, f_M was almost two-fold higher in the green plant compared to that of the etiolated state.

5.1.3.2 Determination of the mobile and immobile components

Lacking pure single components for the analysis of the two-component 5-SASL spectra (see Section 2.2.2), we had to isolate them from the composite lipid–protein spectra. This was done in pairwise intersubtraction by making use of the fact that subtracting two-component spectra, with different contributions from the single components, from each other can mutually eliminate the components they contain in smaller proportion [131].

First, the two spectra that were most extreme concerning A_{max}, and consequently A_{min}, hyperfine splitting values were identified. For this, the set of spectra recorded in

different stages of greening at 34 °C was checked since the two-component nature of the spectra was most pronounced at this temperature. Let D_1 and D_2 refer to these spectra with most immobile and mobile character, respectively. These are superpositions of two, yet unknown, mobile (D_m) and immobile (D_i) spectra, thus, one can write

$$D_1 = f_{1m} * D_m + f_{1i} * D_i \tag{5.1}$$

$$D_2 = f_{2m} * D_m + f_{2i} * D_i \tag{5.2}$$

where f_{jm} and f_{ji} are the fractions of the total integrated intensity of the mobile (D_m) and immobile (D_i) components in the corresponding experimental spectra D_j (with $j = 1, 2$), and m and i stand for mobile and immobile components, respectively. Here all spectra are normalized to unit integrated intensity, i.e. they represent the same number of spins. As the spectra consist of these two components only, it holds that

$$f_{jm} + f_{ji} = 1. \tag{5.3}$$

Since D_1 and D_2 were selected so that they display largest and smallest effective outer splittings (i.e. $2A_{max}$), respectively, we can write that $f_{1i} > f_{2i}$ and consequently $f_{2m} > f_{1m}$. Performing the following mutual subtraction on Eqs. 5.1 and 5.2, one obtains that

$$D_i * (f_{1i} - f_{2i} * \frac{f_{1m}}{f_{2m}}) = D_1 - \frac{f_{1m}}{f_{2m}} * D_2 \tag{5.4}$$

$$D_m * (f_{2m} - f_{1m} * \frac{f_{2i}}{f_{1i}}) = D_2 - \frac{f_{2i}}{f_{1i}} * D_1. \tag{5.5}$$

Note that pure immobile and mobile spectra appear on the left sides of Eqs. 5.4 and 5.5. Normalizing these spectra again to unit second integral results in D_i and D_m.

Since the factors f_{ji} and f_{jm} were not known, these subtractions were performed interactively by changing only the subtraction factors until normal single component lineshapes were obtained for D_i (Fig. 5.8, trace B) and D_m (Fig. 5.8, trace C). These subtractions were judged visually, but an independent test for the consistency and the quality of subtractions was that all the spectra, other than D_1 and D_2, could be constructed as the linear combination of D_i and D_m. As can be seen in Fig. 5.8, excellent fits could be obtained using the D_i and D_m components found using the above intersubtraction technique. The immobile fractions (f_i) were determined by the optimization procedure since they were the only fitting parameters in addition to small horizontal shift between the components.

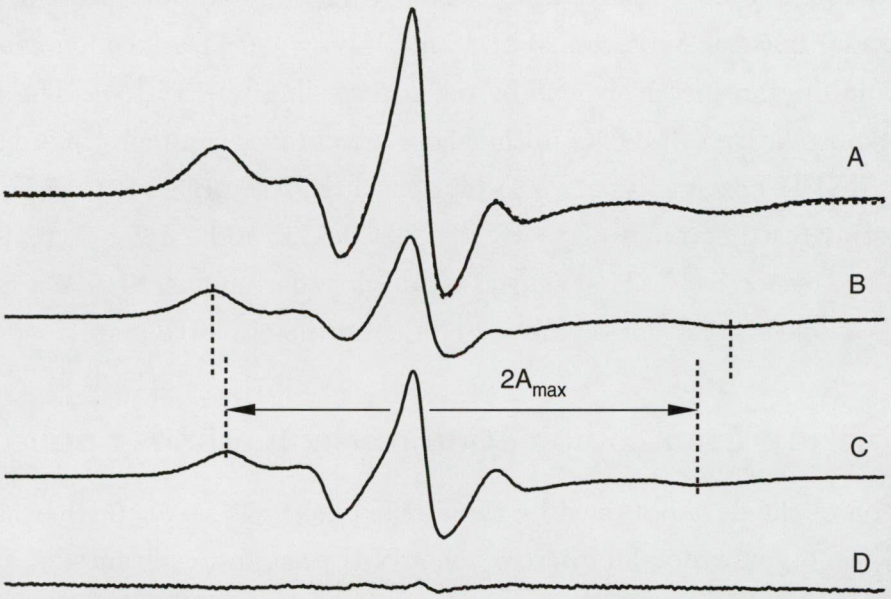

Figure 5.8: ESR spectrum of 5-SASL in etiolated thylakoid membrane recorded at 34 °C (A, dashed line). The spectrum was decomposed into immobile and mobile components (B and C, respectively) by spectral subtraction. The component spectra are scaled to represent their fractional weight in the experimental composite spectrum. The best fitting weighted sum of the components is shown together with the experimental spectrum (A, solid line). (D) is the residual.

5.1.3.3 Rearrangement of the lipid–protein interface

The values of immobile fraction (f_i) obtained by applying the above intersubtraction technique on the 34 °C spectra of 5-SASL, aided with non-linear least-squares optimization were 58%, 58%, 74%, 59%, and 38% (±2%) for 0, 6, 12, 24, and 48 h of greening, respectively. The big change in f_i during greening, at constant lipid/protein ratio (n_t) and lipid headgroup composition [98], can only be explained if changes in the intramembranous size of protein assemblies are assumed. Let have, for simplicity, membrane proteins the same size. The number of interfacial lipids per monomer protein (N_b) is related to the number of monomers in the protein assembly (oligomer), due to the exclusion of lipids from protein–protein contact regions. A simple model [131, 132] can be used to estimate the relative mean oligomer dimensions of these proteins from f_i [58, 133]. Assuming circular intramembranous intersection for both lipids and proteins of an $n * n$ oligomer, N_b is reduced approximately by $1/n$ relative to that of a single monomer (for $n > 1$), neglecting lipid-trapping sites unavailable for bulk lipids and the label. The change in the mean diameter of oligomers relative to that of the monomer (i.e. n) can be estimated from the change in N_b according to Eq. 2.2 on page 13 (where K_r is the association constant

of SASL relative to the host lipid). n_t is obtained from the assayed protein/lipid ratio. A mean molecular mass of $MW_p = 623$ kDa and $MW_l = 0.9$ kDa for monomeric protein (assemblies) and lipid, respectively, can be taken according to [132,134]. The association constant of SASL relative to MGDG in thylakoid membranes can be estimated from that of SASL and MGDG observed relative to phosphatidylglycerol [89,131] to be $K_r \approx 6.5$. With these estimates the values of n are 1.0, 1.1, 0.6, 1, and 2.7 for 0, 6, 12, 24, and 48 h of greening, respectively. That is, the mean oligomer number (i.e. $n * n$) increases significantly (≈7-fold) in mature thylakoid relative to the etiolated state.

5.1.4 A picture from combination of the methods applied

The comparison of the data obtained by the applied methods serves further useful information about the organization and development of thylakoid membranes.

Since f_M and $\nu_{sym}CH_2$ are to increase upon increasing fluidity [25,84], the upward shift in $\nu_{sym}CH_2$ (Fig. 5.2) and the simultaneous drop in f_M (Fig. 5.5) above 45–48 °C demands explanation. For the interpretation of these data, it should be emphasized that the major lipid of these membranes is monogalactosyl diacylglycerol (MGDG) (with polyunsaturated acyl chains [132,135]) which adopts an inverted hexagonal (H_{II}) phase under normal conditions [22,136–138]. Thus, MGDG is forced into a lamellar structure in thylakoids [139]. $\nu_{sym}CH_2$ is rather high (≈2854 cm^{-1}) in the non-bilayer (H_{II}) phase of MGDG [25]. Considering the similar values obtained after the sharp increase in $\nu_{sym}CH_2$ above 48 °C (Fig. 5.2), the transition can only be interpreted as the formation of the H_{II} phase by MGDG in agreement with [53,140,141]. It also explains the decrease in f_M (Fig. 5.5) assuming that TEMPO partitions badly into the H_{II} phase of MGDG because of the tightly packed headgroup region in this structure [25]. Comparing with $\nu_{sym}CH_2$ and f_M, the order parameter, S, calculated from 5-SASL spectra did not show similar changes above 45–48 °C upon heating. One should remember, however, that the nitroxyl group of 5-SASL is located on C-5, hence it monitors acyl rotational dynamics close to the polar–apolar membrane interface.

It can be seen in Fig. 5.2 that the exclusion of MGDG happened ≈16 °C higher than partial protein unfolding after 12 h of greening. This difference decreased to 4–5 °C for the green plant due to an improved heat stability of newly synthesized/assembled thylakoid proteins, a further increase in the 18:3 acyl chains and probably stronger protein–lipid structural coupling. The exclusion of MGDG (and formation of non-bilayer phase) seems therefore to be initiated by thermal unfolding of proteins. The increased heat stability of thylakoid proteins during greening is accompanied by an increase in the relative amount of α-helix and β-sheet structural forms on the cost of less regular structures and by a decreased fraction of immobilized lipids, and thus, by an increase in the mean oligomer

number, which are in good agreement with a loss in ELIPs and a large gain in LHCII indicated by SDS PAGE (see Section 5.1.1). (It is known that LHCII is in the monomeric form in the early phases of greening, and later oligomers and large arrays are formed [104]). Moreover, a lower lipid packing (increased mobility) developed in the mature membrane as indicated by TEMPO. It is in agreement with the increasing amount of polyunsaturated fatty acids during greening.

Earlier, Mysliwa-Kurdziel *et al.* suggested at least two phases of greening [142]. Our data on thylakoid development can be interpreted as a sequence of correlated molecular events grouped into three phases. Greening starts with the onset phase (0– 6 h), where the Chl content increases at a very low rate, LHCII apoproteins are almost absent but ELIPs have their maximum density in the SDS PAGE. The heterogeneity concerning proteins is largest in the rearrangement phase (6–24 h), where approximately 67% of the total Chl content is gained and a large increase of the 18:3 fatty acid content can be observed. Formation of larger and more stable protein assemblies occurs in the maturation phase (24–48 h), where, in agreement with [104], LHCII apoproteins dominate the SDS PAGE and the Chl accumulation saturates. It should be noted here that the precise time course of the underlying processes depends on the environmental conditions, such as the intensity of illumination, light quality, water supply, humidity which could influence the overall time course and the manifestation of the three phases. Our experiments showed that this was most noticeable in the early phases of greening, before 12 h in particular. After 12 h, however, the greening process always followed the same way, which is obviously required for the establishing of the functional membrane.

In conclusion, the protein–lipid interaction and the fluidity of the thylakoid membrane are determined to a large extent by changes in protein assemblies and progression of fatty acid desaturation. The latter is important for the control of overall membrane fluidity and the non-bilayer propensity of MGDG. It appears that a structurally balanced interplay between major protein and lipid components develops gradually into a fully functional organization in mature thylakoid. This process allows rearrangement of protein–protein and protein–lipid interactions, hence adaptation to external conditions during development, and serves both structural flexibility and stability.

5.2 New insight into the C–H stretching region of lipids

In model and in biological membranes as well, FTIR spectroscopy has been widely used to investigate acyl chain conformations [11, 26]. The most frequently utilized infrared spectroscopic parameter in these systems, as it was mentioned in Section 2.1.1, is the frequency of the symmetric CH_2 stretching mode near 2850 cm^{-1}. In Section 5.1.2, it was shown how the $\nu_{sym}CH_2$ band served as a reporter on membrane structure and dynamics in our experiments. In spite of this and many other successful applications dealing with this band, some questions still remained to be answered. In our band fitting analyses of the $\nu_{sym}CH_2$ bands, a small but systematic error could be observed at low temperatures which disappeared upon heating, i.e with increasing number of disordered segments in lipid acyl chains. Therefore, the questions raised up: what is behind this phenomenon and what is the precise mechanism behind the temperature dependence – the frequency shift in general – of νCH_2 bands. That is why we tried to obtain more information on the C–H stretching bands in the FTIR spectrum.

If the origin of the broadening and upward shift of the νCH_2 bands in more disordered systems or at elevated temperatures is to be understood, two possible factors must be separated. One possibility is that the bands are shifting due to changing force constants between the involved C and H atoms (similarly what happen to C=O bonds in hydrogen bonding). In this case, the frequency of the νCH_2 vibrations might be more characteristic of the intermolecular effects than of the molecules themselves. The other possibility is that the frequency of a νCH_2 vibration is more determined by the conformation of the hydrocarbon chain, with slightly different frequencies for ordered and disordered segments. In this case, the observed frequency shift and broadening of the apparent νCH_2 bands can be the results of competing component bands, whose intensities are changing in accordance with the changes in the ordered and disordered segment populations. This second case, however, demands a proof of a prerequisite: The frequencies of the C–H vibrations are characteristic basically of the conformation of the chain in which they are situated and are rather insensitive to environmental effects. Therefore, we were looking first for a model system in which the interchain effects can be separated from the intrachain conformational effects.

5.2.1 Noncooperative fatty acyl chains in lipid membranes

DOPC vesicles were saturated to different extents in a homogeneous catalytic reaction in a deuterium-containing environment. In consequence of the presence of deuterium gas in the catalytic reaction, the C_9 and C_{10} of the oleoyl chains became deuterium-labelled upon saturation. Since the catalytic reaction was always interrupted, a different mixture

of DOPC, OSPC, SOPC and DSPC molecules was created in each case. From the mixtures obtained after 0% (pure DOPC), 28%, or 45% saturation of the DOPC oleoyl chain double bond, multilamellar systems were prepared to study the characteristic features of their νCD and νCH_2 vibrations.

This system had unique features. Mixtures of lipids obtained upon saturation of DOPC with deuterium to different extents were homogeneous as concerns the CD groups, since these groups were present only in saturated hydrocarbon chains, and all were in the same position along the chains. On the other hand, the deuterated DOPC mixtures were heterogeneous regarding CH groups. The mixtures contained 0%, 28%, or 45% saturated fatty acyl chains, and the increasing presence of the saturated chains rigidified the membranes.

Indeed, as the level of saturation increased, the observed maxima in the $\nu_{sym}CH_2$ and $\nu_{as}CH_2$ stretching bands at around 2853 and 2924 cm^{-1} downshifted by 2 and 6 cm^{-1}, respectively (Fig. 5.9A). When only oleoyl chains were present in the lipids, the multil-

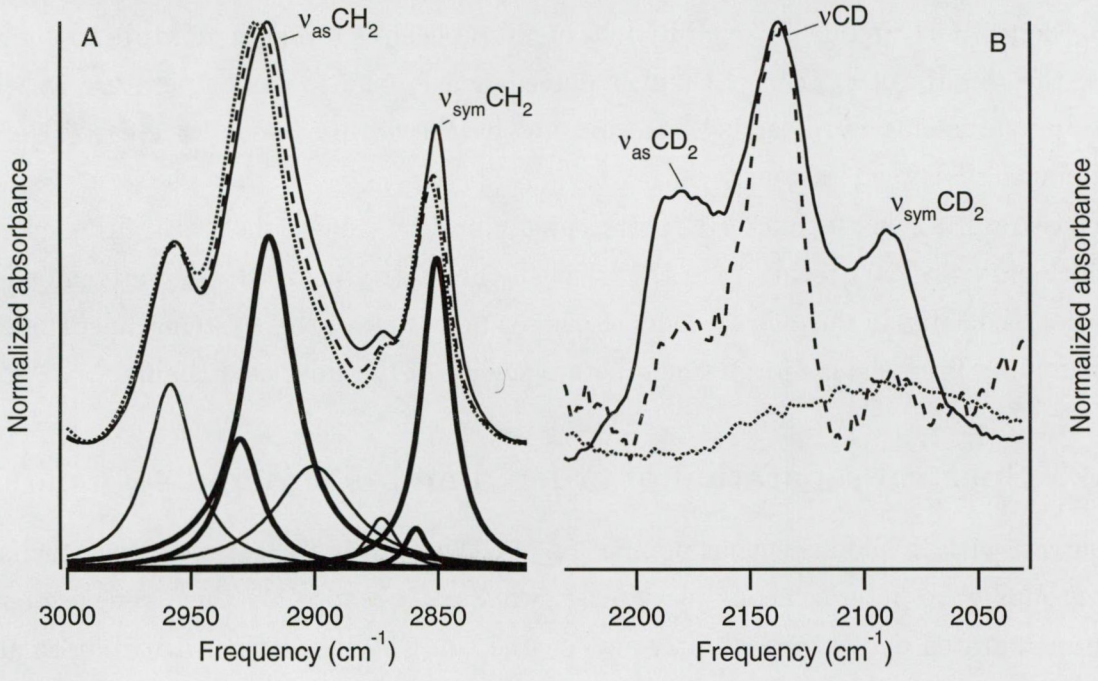

Figure 5.9: The CH (A) and CD (B) stretching region of catalytically deuterium-saturated DOPC multilamellar systems at room temperature. Levels of saturation of the oleic acyl chains: (···) 0%; (- -) 28%; (—) 45%. The lower set of curves in panel A are the fitted Lorentzian component bands, which were at 2958 cm^{-1}; 2930 and 2918 cm^{-1} ($\nu_{as}CH_2$); 2899 cm^{-1}; 2873 cm^{-1}; 2853 and 2850 cm^{-1} ($\nu_{sym}CH_2$). Thicker lines indicate νCH_2 components. For complete assignment, see Table I in Annex III.

amellar system was in the liquid-crystalline phase at room temperature, characterized by high $\nu_{sym}CH_2$ frequencies. At the same room temperature, however, the saturated stearoyl chains formed in the catalytic reaction at the expense of the oleoyl chains were not melted.

In a homogeneous dispersion, stearoyl chains would form a rigid gel phase characterized by low $\nu_{sym}CH_2$ at room temperature [26]. Thus, the presence of more stearoyl chains in the lipids made the system more rigid, which was reflected by a downshift in the νCH_2 frequencies.

In contrast, the νCD band (Fig. 5.9B) did not shift upon increasing saturation, that is, the changing environment had no effect on this vibration: $\nu CD = 2136 \pm 0.2$ cm^{-1} for both 28% and 45% saturated mixtures.

It should be mentioned here that the presence of the unexpected CD_2 groups was a consequence of the particular behaviour of the catalyst. It is important that CD_2 groups could be present only in the previously unsaturated segment of the fatty acyl chain. The details of this phenomenon are discussed in [143]. Thus, although the $\nu_{sym}CD_2$ frequencies ($\nu_{sym}CD_2 = 2089 \pm 3$ cm^{-1} for the 28%, and 2088 ± 0.3 cm^{-1} for the 45% saturated mixture) were determined with higher error due to the lower signal-to-noise ratio, they could be used to characterize the chain conformation. The value of 2088 cm^{-1} for $\nu_{sym}CD_2$ corresponds to gel phase lipids (for comparison see, for example, [144]). Like νCD, the $\nu_{sym}CD_2$ frequency exhibited no measurable shift from one mixture to another. Thus, the rigidity of a stearoyl chain is determined by the room temperature at which these measurements were carried out, and not by the nature (oleoyl or stearoyl) of the neighbouring fatty acyl chains.

These results suggest that CH(D) stretching vibrations reflect the state of the molecule of which they are part rather than the effect of the matrix in which they are embedded. The observed shifts in the νCH_2 frequencies here and in many other systems must therefore result mainly from the conformational heterogeneity of the lipid acyl chains.

5.2.2 Spectral separation of ordered and disordered segments

In contrast with the homogeneous population of CD groups in the saturated oleoyl chains, CH_2 groups were heterogeneous in at least two ways, because (1) they were present in both unsaturated and saturated fatty acyl chains, and (2) due to their distribution along the fatty acyl chains. The frequency shift in the νCH_2 bands must therefore result mainly from the changing populations of different conformers present in the system.

The above heterogeneity was represented with only two components as a first approximation. Indeed, as shown in the lower part of Fig. 5.9A for the 45% saturated mixture, two components could be fitted to both the $\nu_{sym}CH_2$ and the $\nu_{as}CH_2$ bands of these lipid mixtures. As the level of saturation increased, so did the intensity ratio of the $\nu_{sym}CH_2$ components, I_{2850}/I_{2853}. It was $\approx$0 at 0%, 0.13 at 28%, and 0.33 at 45% saturation. The other conformation-sensitive band, $\nu_{as}CH_2$, behaved similarly, exhibiting two components at 2918 and 2930 cm^{-1} with intensity ratios of 2.5, 4.6, and 9.6 at 0%, 28% and 45%

saturation, respectively. (It should be noted here that the differences in the absolute values of the intensity ratios of the $\nu_{sym}CH_2$ and $\nu_{as}CH_2$ components may be caused by the more complex structure of the region around the $\nu_{as}CH_2$ band.) Since we know that lower frequency corresponds to more ordered acyl chains, we assign the lower-frequency components of the νCH_2 bands to the CH_2 groups situated on the more ordered segments, while the higher-frequency components of the νCH_2 bands to the CH_2 groups of the more disordered segments of the fatty acyl chains.

Since the experiments involving DOPC and its deuterium-saturated derivatives were carried out at room temperature, the changes in the populations of the ordered and disordered fatty acyl chain segments originated from the increasing level of saturation of the mixtures. Physically, it is a different problem when the ordered and disordered segment populations in a chemically homogeneous system are shifted by an increase of temperature. Nevertheless, if the assignments to the ordered and disordered segments are correct, the same reasoning should be able to describe the temperature-affected conformer populations as well. For the study of temperature-induced conformers, hydrated DPPC multilayers were chosen.

5.2.3 Temperature-induced changes in model membranes

When using curve fitting procedures, one frequently expressed concern is whether these provide unique solutions. While we did not encounter such a problem with our curve fittings, we were looking for a mathematically more exact approach to demonstrate the existence of two oppositely changing component bands which can describe the observed νCH_2 frequency shifts. The method chosen was SVD (see Annex III and [119]). This involves an algorithm which does not require preliminary assumptions; it uses only the data set represented by the experimental spectra recorded during the change of an external parameter. The first n_s SVD basis spectra contain the linearly independent variables from which the original spectra (neglecting the noise of the experiment) can be reconstituted [119].

The SVD analysis was carried out on 27 spectra of DPPC multilayers recorded between 5 and 65 °C. Since the intensity of the third and higher SVD components was very small, we treated the two most significant SVD basis spectra. The first basis spectrum (Fig. 5.10A), which represents the common part of all spectra in the set, could be fitted very well by freely optimized Lorentzian component bands. The second basis spectrum reflects the spectral change accompanying the presence of an increasing number of disordered fatty acyl chain segments upon heating (Fig. 5.10B). It had derivative-like structures around the νCH_2 bands, with positive loops on the high-frequency sides. It can be seen that this basis spectrum can only be fitted by assuming a minimum of two components in the

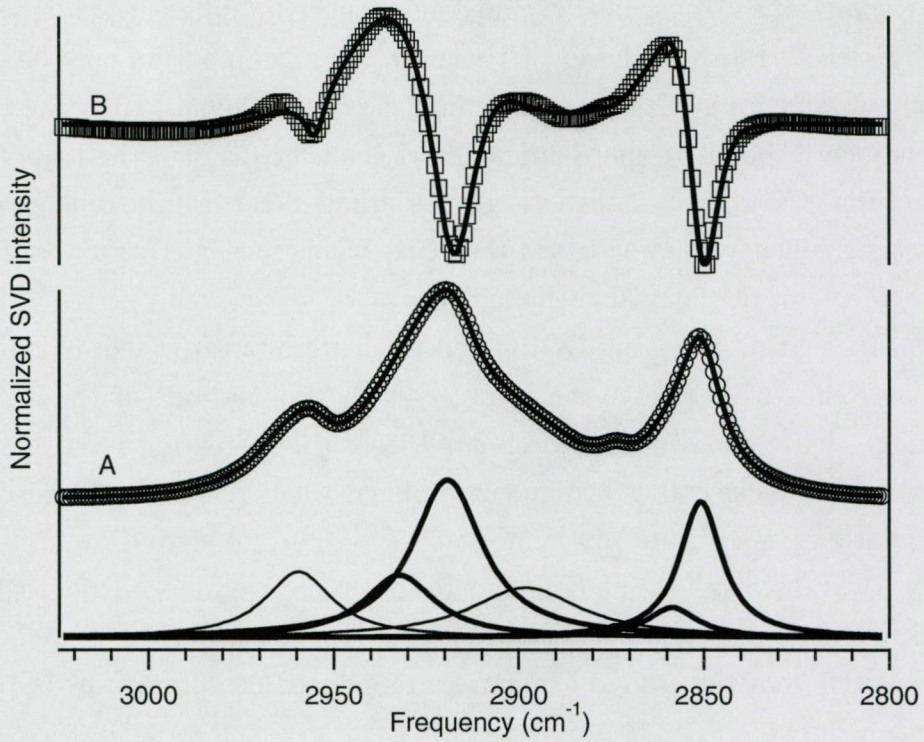

Figure 5.10: The first (A) and the second (B) SVD basis spectra calculated from 27 DPPC spectra recorded between 5 and 65 °C. Continuous lines through symbols show the fitted curves, optimized for the first SVD basis spectrum. The parameters of the first fit were then fixed during the fit of the second basis spectrum, with the exception of the intensities. Component bands drawn with thicker lines are the components of the $\nu_{sym}CH_2$ and $\nu_{as}CH_2$ bands. SVD components are normalized and shifted for clarity.

νCH_2 regions. Indeed, a very good fit was obtained for both the first and the second basis spectra with two Lorentzians for the νCH_2 bands. The consistency of the fit was justified by the fact that the second basis spectrum could be fitted with exactly the same components as used for the first basis spectrum, but allowing only their intensities to be varied during the fit. That is, the spectral change as represented by the second basis spectrum can be described by an increase in the higher- and by a decrease in the lower-frequency component bands, exactly the same ones as found for the first basis spectrum. The good fit underlines that the frequency shift observed for $\nu_{sym}CH_2$ upon heating can be described by the competition of two components, representing ordered and disordered segments of the acyl chains.

Afterwards, for analysis of the population changes in the ordered and disordered segments, only the intensities of the component bands were fitted to each of the 27 experimental spectra. The temperature dependencies of the 2851 and 2859 cm^{-1} component band intensities are shown in Fig. 5.11. It can be seen that at low temperatures only the 2851 cm^{-1} component was present, since the intensity of the 2859 cm^{-1} component

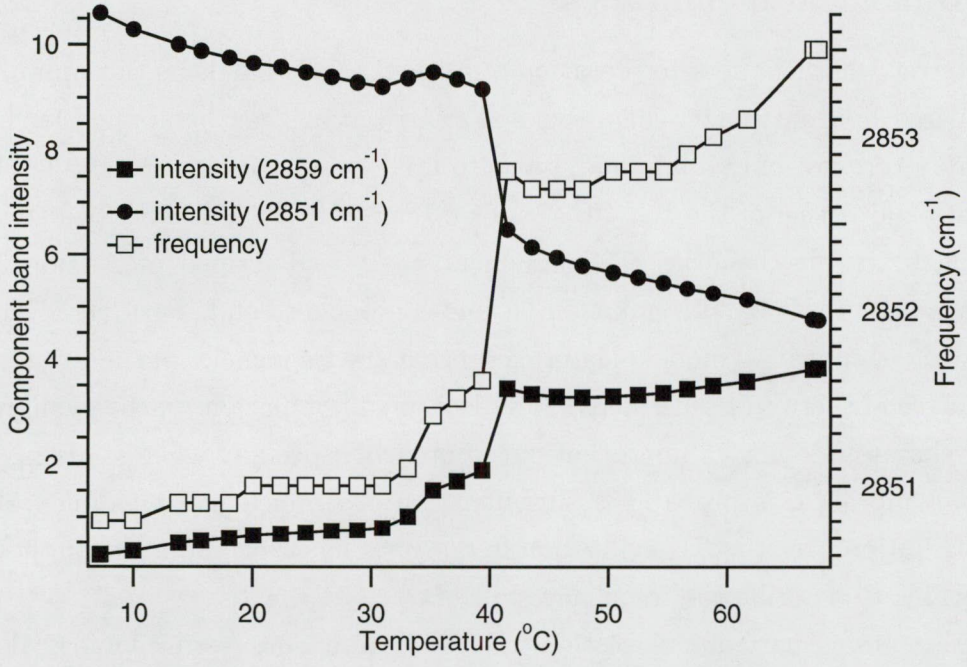

Figure 5.11: Gel to liquid-crystalline phase transition of DPPC multilamellar system. (□) Shift in $\nu_{sym}CH_2$ obtained by plotting frequency versus temperature with a single Lorentzian fitted to the $\nu_{sym}CH_2$ band. This curve pertains to the right y axis. Intensities of the 2851 (●) and 2859 cm^{-1} (■) component bands of $\nu_{sym}CH_2$ obtained from SVD analysis. These curves pertain to the left y axis.

was negligible here. Its intensity became considerable only in the pretransition region, at around 32–40 °C (Fig. 5.11). At the gel to liquid-crystalline phase transition at around 41 °C the intensity of the 2859 cm^{-1} component band abruptly increased, while that of the 2851 cm^{-1} component band decreased. This shift toward the disordered conformers is the underlying process of the frequently utilized frequency shift in $\nu_{sym}CH_2$ in monitoring lipid phase transitions (Fig. 5.11, □).

This approach also can explain the origin of the earlier observed increase in the $\nu_{sym}CH_2$ bandwidth upon phase transition [25]. In the liquid-crystalline phase, both component bands (at 2851 and 2859 cm^{-1}) are present under the contour of the $\nu_{sym}CH_2$ band of the IR spectrum, and its width is therefore necessarily larger here than in the gel phase, where only the 2851 cm^{-1} component dominates. The presence of two changing components also can explain the nonconcerted temperature dependence of the width and the frequency of the $\nu_{sym}CH_2$ band reported by several authors [144–147]. The width is more sensitive to the appearance of the second, close-lying component band than the frequency, especially if the frequency is determined from the topmost five data points [145]. In this case, the second component must possess a considerable intensity before measurably affecting the peak position. Furthermore, using this two-component method, the systematic error mentioned on page 34 cannot be observed.

5.2.4 Biological membranes

It is of interest whether the interpretation of lipid $\nu_{sym}CH_2$ bands as the sum of ordered and disordered lipid fatty acyl chain segment contributions can be applied for biological membranes where not only lipid–lipid, but also lipid–protein interactions take place.

Indeed, band fitting of the $\nu_{sym}CH_2$ bands of barley thylakoids with two components also gave a better fit than the one-component analysis described in Section 5.1.2. It suggests again that this band is not a simple one-component band. Further, SVD analysis also revealed – similarly to model membranes – that the frequencies of the $\nu_{sym}CH_2$ bands can be analysed in terms of the ordered and disordered populations of the membrane lipid fatty acyl chains. Keeping in mind that our approach, especially when studying complex biological membranes, is probably a simplification of a much more complex behaviour of the distribution over the CH_2 vibration frequency, the two-component method proved well applicable to describe the frequency shift of $\nu_{sym}CH_2$ bands.

In the remaining part of this section, the study of an interesting biological problem will be discussed, where this two-component approach turned out to be very useful.

Tobacco thylakoid membranes

The importance of PG in chilling sensitivity was briefly described in Section 2.3. It was shown earlier that the chilling sensitivity of tobacco can be altered by genetic manipulation of the fatty acid unsaturation of PG [114]. We used practically the same wild-type and genetically manipulated tobacco plants to study the role of PG in protein–lipid interactions and membrane dynamics. The application of complementary DNAs (cDNAs) for glycerol-3-phosphate acyltransferases (GPATs) from squash and *Arabidopsis* resulted in the level of *cis*-unsaturated fatty acid content in PG molecules being lower (12 mol%) in the squash (TOSQ), and higher (36 mol%) in the *Arabidopsis* transformants (TOAR), as compared with the wild-type tobacco (32 mol%) (TOBA) [114]. Thus, the chilling sensitivities of the transformed tobacco plants changed in accordance with the character of squash and *Arabidopsis*, respectively [114].

The C–H stretching regions of the IR spectra, involving contributions mostly from the fatty acyl chains of the membrane lipids, were very similar in the three plants (see Fig. 5.12 for the TOBA spectrum). Nevertheless, the $\nu_{sym}CH_2$ band for TOSQ was at somewhat lower frequency, indicating more ordered fatty acyl chains here as compared with TOBA and TOAR. According to the separation approach, we fitted two components to the $\nu_{sym}CH_2$ bands. Let O and D refer to the components representing ordered and disordered fatty acyl chain segments, respectively (Fig. 5.12).

It should be borne in mind that in our approach – as mentioned above – the decomposition of the $\nu_{sym}CH_2$ band into only two components probably is an approximation,

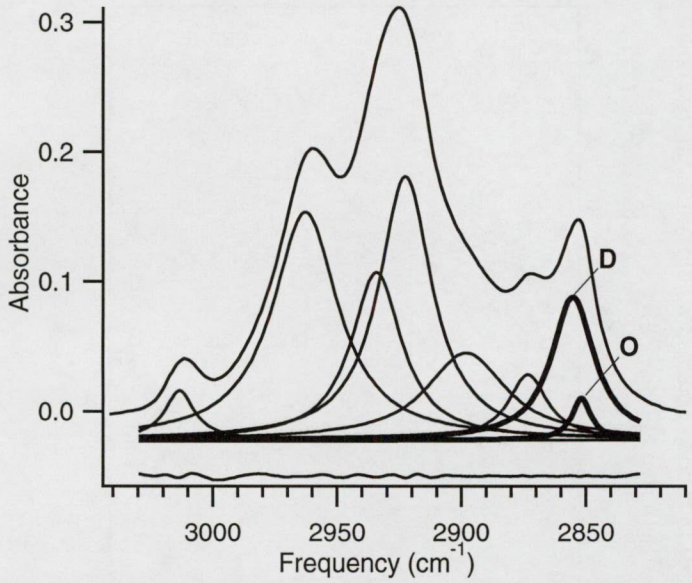

Figure 5.12: Decomposition of the C–H region as demonstrated on thylakoid membranes of TOBA. Component bands are depicted on the calculated constant background needed for the fit. The *O* (ordered) and *D* (disordered) components are drawn with thicker lines. Spectrum was taken at 5 °C. Residuals are displaced for clarity.

and the signal-to-noise ratio and the number of data points do not allow more meaningful distinctions. As a further simplification of the situation, we assumed that molecules could be ordered only one way. Therefore, we did not consider any variability for the *O* component band. In contrast, the disordered state of the fatty acyl chains is not regarded as a well-defined, unique state, but it has conformational distribution, and this distribution may change with increasing temperature. Thus, for the fitting of a series of spectra recorded as a function of increasing temperature, the strategy was as follows: Since the *O* component may be expected to 'melt' away with increasing temperature, the parameters of the *O* component (frequency and width) were kept constant after their determination from spectra recorded at 5 °C. The *O* component was most intensive at this temperature, and thus its parameters could be determined with the highest accuracy here. This approximation does not allow distribution over different conformations for the *O* component. In contrast, all parameters of the *D* component (representing disordered segments) were left free. To permit the comparison of different experiments, each spectrum was normalized with the integral of its fitted region (e.g. 2820–3050 cm^{-1} for C–H stretching).

The results of such fits for the thylakoid membranes of the three plants are shown in Fig. 5.13. The ratios of the intensities of the *O* components over the *D* components are given in Fig. 5.13A as a function of temperature. We chose this ratio to aid comparison between different membranes, but it should be kept in mind that it has no detailed molecular structural meaning. As may be seen in Fig. 5.13A, TOBA exhibited only a

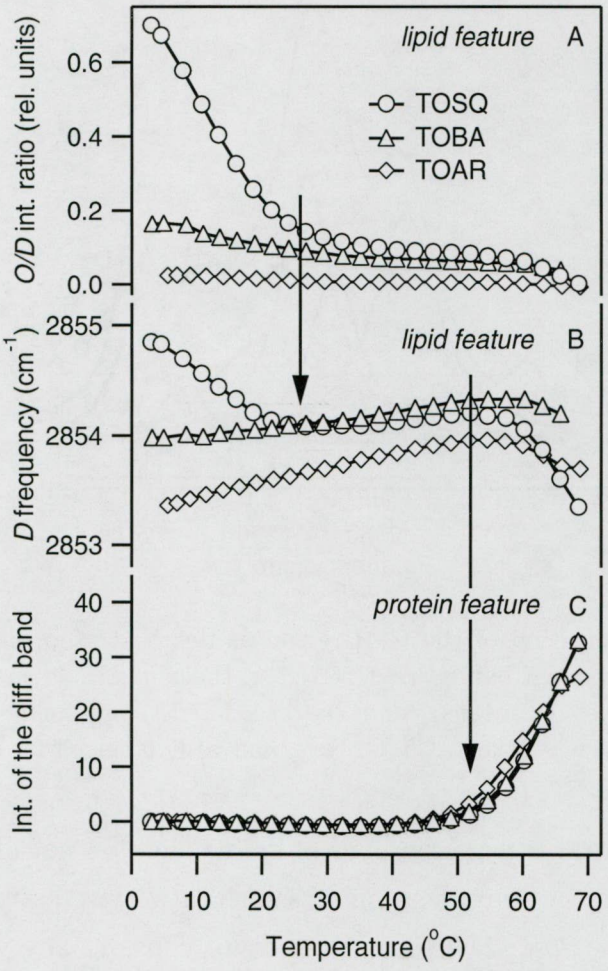

Figure 5.13: Correlation between lipid and protein dynamics in the thylakoid membranes of wild-type and genetically manipulated tobacco plants. (A) Temperature dependence of the intensity ratios of the O and D components of the $\nu_{\mathrm{sym}}CH_2$ band, (B) frequencies of the D components, (C) heat-induced denaturing of the membrane proteins as characterized by the increasing intensity of the difference band at around 1620 cm^{-1} (see Fig. 5.14B).

very slight decrease of the O/D ratio between 5 and 25 °C, and the ratio then levelled off. TOAR exhibited a lower O/D ratio with no breakpoint at all. At low temperatures, the relative amount of the O component was highest in TOSQ. In TOSQ, as shown above, the level of saturated fatty acyl chains in the PG molecules is considerably higher than in TOBA (76% of the PG molecules in TOSQ versus 36% in TOBA). The further slight decrease in the O/D ratios above 50 °C may be related to changes in the structure of the membrane proteins and will be discussed below.

There were considerable differences between the three plants studied in the temperature dependence of the frequency of the D component. This frequency is expected to shift upward with increase of the temperature-induced lipid fatty acyl chain disorder at

higher temperatures. Indeed, there was a tendency to shift toward higher values in the frequencies of the *D* components for all three membranes. It is noteworthy, however, that while the increase in the *D* frequency for TOAR started immediately at 5 °C, for TOBA there was a slightly lower rate of increase up to about 25 °C, and for TOSQ there was a considerable decrease before a slow increase started. It is interesting that changes in the temperature courses of the *D* frequency curves in TOBA and TOSQ coincided with the completion of the 'melting' of the *O* components (see the arrow between Figs 5.13A and 5.13B).

With the constraints of our fitting strategy in mind, the decreasing phase of the $\nu_{sym}CH_2$ frequency of the *D* component in TOSQ can be explained in the following way: At the lowest temperatures, the fatty acyl chains that are disordered are mostly those which interact directly with the proteins. Upon the heat-induced $O \rightarrow D$ transition, fatty acyl chain segments pass from an ordered state to a disordered one, and the distribution of these freshly disordered segments over the possible conformations will not be the same as that in the protein-perturbed fatty acyl chains. The freshly 'melted' distributed population will be 'colder' (i.e. it will have a lower characteristic $\nu_{sym}CH_2$ frequency) than the *ab ovo* existing protein-related disordered lipid fatty acyl chain population. Since we fit only one band to the whole disordered population, the frequency of the *D* component can start to shift upwards only after the $O \rightarrow D$ transition has been completed. As long as the 'melting' of the *O* component supplies fresh disordered fatty acyl chains with lower $\nu_{sym}CH_2$ frequency, the average $\nu_{sym}CH_2$ frequency of the overall *D* population will shift down, stagnate or increase more slowly. These arguments together may prove that the two-component analysis of the $\nu_{sym}CH_2$ band can not only demonstrate the existence of two major CH_2 populations, but also allows the changes within the distribution of the disordered fatty acyl chain segments to be followed to some extent.

The effect of the *O* component melting should be smaller in those plants where the ordered population is expected to be smaller. Indeed, whereas for TOSQ there was a spectacular decrease in the *D* component frequency up to about 25 °C, for TOBA only the rate of increase was somewhat lower up to this temperature, and for TOAR no effect was visible at all (Fig. 5.13B). In this transformant, the amount of *cis*-unsaturated fatty acids in PG is increased as compared with TOBA. Moreover, there was a breakdown in the *D* frequency in each of the three plants in the temperature region of 50–60 °C. If only the fatty acyl chain disorder is considered, such a phenomenon should mean increasing order of the chains in this temperature range. If only lipids were present in the investigated system, such a phenomenon would be impossible. Therefore, the behaviour of proteins should also be investigated, since it is to be expected that their denaturing may occur in this temperature range, affecting the lipid phase.

The magnitude of the difference between the O/D ratios of the wild-type and transformed plants seems at first glance to be too large, especially that between TOBA and TOSQ. Since PG accounts for only about 6–8% of the total phospholipids, changes in the fatty acid composition involve only 3–4% of the total fatty acid content. Nevertheless, we found this difference consequently in several series of experiments, and even the amplitudes of the differences were similar. Further, if it is taken into account that the introduction of the squash GPAT into the tobacco increases the amounts of the 16:0 palmitic acid and the 18:0 stearic acid at the expense of the 18:1, 18:2 and 18:3 *cis*-unsaturated fatty acids [115], the effect on the membrane dynamics should be larger than proportional to the fractions of the affected fatty acids. In themselves, palmitic and stearic acids would be in the gel phase, and the 18:1, 18:2 and 18:3 *cis*-unsaturated fatty acids in the liquid-crystalline phase at 5 °C. Additionally, saturated fatty acids, present in higher amounts in a membrane, may either form separate gel patches or exert a synergic effect on the order of the fatty acyl chains of the other lipids too.

Structure and heat-denaturing of thylakoid membrane proteins. Fig. 5.14 depicts the 1600–1760 cm^{-1} region of the IR spectra of the three tobacco-based plants. The strong

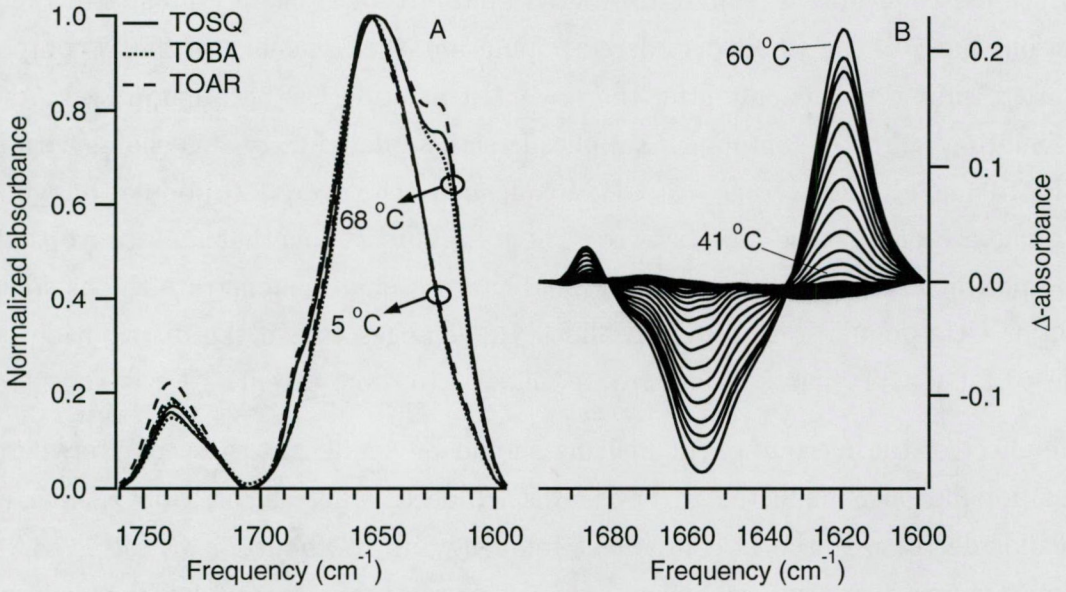

Figure 5.14: (A) Comparison of the spectra of TOBA, TOSQ, TOAR in the amide I and ester C=O stretching region at 5 and 68 °C. (B) Representative heat-induced difference spectra in the amide I region. The differences were calculated from the spectra as shown in Fig. 5.14A by subtracting the spectrum recorded at 5 °C from each spectrum registered at increasing temperatures.

similarity of the three spectra recorded at 5 °C indicates that, as intended, the genetic manipulation affected only the fatty acid composition of the membranes, the protein components remaining unchanged. On increasing temperature, heat-denaturing occured

involving the appearance of a strong and a weaker band, at around 1620 and 1684 cm^{-1}.

For a detailed characterization of this process, difference spectra were calculated by subtracting the first spectrum of a temperature run from those recorded at increasing temperatures (Fig. 5.14B). The source of the noteworthy parallel evolution of the 1620 and the 1684 cm^{-1} bands, which are characteristic of intermolecular β-structures [52,53], was the degradation mostly of α-helices, as shown by the deepening of a negative band at around 1658 cm^{-1}.

To quantify the progress of heat-denaturing, a Lorentzian curve was fitted to the 1620 cm^{-1} band emerging in the difference spectra. The intensities of this band as a function of temperature for TOSQ, TOBA and TOAR are plotted in Fig. 5.13C. To allow a comparison of the different plants, before calculation of the difference spectra each spectrum was normalized with its own intensity integrated between 1594 and 1700 cm^{-1}. Thus, the intensity of the 1620 cm^{-1} difference band can be directly related to the denatured fraction of the membrane proteins. Therefore, the thermotropic responses of its intensities can reveal the differences between the three plants in respect of the denaturing of their thylakoid membrane proteins. According to Fig. 5.13C, the proteins in the TOSQ, TOBA and TOAR thylakoid membranes denatured in very similar ways. (To illustrate the variability between plants grown at different times, two different series are shown in Fig. 5.14A and Fig 5.13C. That is the reason why the extents of protein denaturing are somewhat different in Fig. 5.14A and Fig. 5.13C, for the three tobacco-based plants as compared to each other at around 68 °C.) The identical heat-stabilities of the proteins in spite of the different fatty acid compositions of the PG molecules may mean that other lipids are indeed responsible for the maintenance of protein stability. At the same time, however, PG molecules may have the important role of 'filling up' fragmented places at the protein–lipid interface; the small size and the charge of their headgroup would make such a role feasible. This function can be affected selectively and to a large extent by introducing genetically manipulated PG molecules into an optimized system.

Comparison of the temperature of onset of the protein denaturing in Fig. 5.13C and the temperature of onset of the high-temperature decline of the D component frequencies in Fig. 5.13B reveals a coincidence between them (indicated by an arrow). Thus, a purely lipidic feature of the IR spectrum could be correlated with a purely proteinic feature. The facts that protein denaturing involves major rearrangement in the thylakoid membranes, and that it affects lipid disorder, can be explained with the appearance of protein aggregates which results in a smaller surface available for protein–lipid interactions. Therefore, some lipids have to dissociate from the proteins, and in their own phase, these lipids may form domains in which they are less disordered than they were at the protein–lipid interface. This means a lower average frequency for the D lipid component,

with the frequency downshift starting at around the same temperature as that for protein denaturing (Fig. 5.13B).

The role of PG molecules in functioning of thylakoid membranes has been shown in different studies [107–109], however, in none of these works were the stability and the dynamics of the involved protein components studied. Our conclusion that PG molecules are probably in close but 'noninvasive' contact with the proteins, and thus participate in the fine-tuning of their working conditions, fits well into the picture indicated so far by biochemical methods.

We observed differences between TOSQ and TOBA only in those parameters which were related to the membrane dynamics, and only at temperatures lower than 25 °C. Accordingly, we suggest that differences should be found between the two plants only under conditions that involve temperatures considerably lower than 25 °C. Indeed, Moon *et al.* [115] detected differences between tobacco and its squash GPAT-transformed mutant only in the sensitivity to low-temperature photoinhibition and in the speed of recovery from the photoinhibited state. Their low-temperature photoinhibition experiments involved the exposure of the plants to 1 °C, where the dynamic properties of the TOSQ and TOBA thylakoids are considerably different (Fig. 5.13A). The extent of photoinhibition was larger and the rate of recovery was lower in the squash cDNA-transformed TOSQ mutant with more rigid thylakoid membranes at low temperatures as compared to those of TOBA. Thus, processes involving larger-scale rearrangements in the thylakoid membrane, such as insertion and processing of the D1 protein (regarded as crucial steps in the recovery process), most probably encounter more difficult conditions in the transgenic plant, and this is the reason for the lower recovery [115]. There is a recent example in the literature for rice that supports the role of saturation/unsaturation of PG discussed above. Manipulating the membrane dynamics in the opposite direction as we did, i.e. increasing the unsaturation of fatty acids in PG via transformation with *Arabidopsis* or spinach GPAT cDNAs, the rate of photosynthesis and growth at low temperatures increased in the transgenic rice seedlings [148].

In conclusion, the introduction of PG molecules via the transformation of tobacco with squash GPAT cDNA led to measurable changes only in the dynamics of the membrane lipids, and only in the low-temperature region, 5–25 °C; the membrane proteins were not affected. The PG molecules of transgenic origin probably accumulate at the protein–lipid interfaces of the thylakoid membrane of the transformed plant. Therefore, any physiological consequence of the squash GPAT gene expression in tobacco should be related to processes depending on lipid dynamics in the low-temperature range.

Chapter 6

Summary

Methodological achievements

1. Development of a spectrum simulation and fitting program for the use of TEMPO spin-label was carried out. With the program, the partition of TEMPO between the aqueous and the hydrocarbon phase of the membrane can be precisely determined, thus providing data on lipid packing and membrane fluidity. Furthermore, the rotational dynamics of TEMPO can also be characterized.

2. It was shown that the $\nu_{sym}CH_2$ band can be resolved into two components, one related to the ordered, the other to the disordered segments of the hydrocarbon chains of lipids, and that the apparent temperature-induced frequency shifts of this band can be described by the competition of its two close-lying components. The method was applied on complex biological membranes as well.

Resolution of biological problems

Greening of barley thylakoids – a model for self-organising a functional biomembrane

3. An intersubtraction method was applied on the ESR spectra of 5-SASL spin-label. It provided an immobile and a mobile component spectrum which could be used to determine the immobilized lipid fraction in barley thylakoid membranes.

4. It was suggested that a structural coupling between major lipid and protein components develops during greening. The fatty acid composition and the stability of the newly synthesized light-related proteins was found to be changing in a concerted way – the appearance of more and more unsaturated lipids provides an appropriate environment for the formation of photosynthetically active protein assemblies with higher stability.

5. The formation of large protein complexes – most of them probably related to LHCII – was followed. It was shown that the mean oligomer size of the proteins increases about 7-fold during greening.

6. Three phases was proposed for the interpretation of the sequence of correlated molecular events during greening. In agreement with the Chl accumulation, greening starts with the onset phase which is followed by the rearrangement phase where the largest changes occur. The functional membrane is formed in the maturation phase.

7. The partial heat-denaturation of protein complexes seems to promote a large-scale lipid structural change in the thylakoid membrane – probably due to a lamellar to inverted hexagonal phase transition of the MGDG lipid species.

Genetically manipulated tobacco thylakoids

8. With the use of the two-component analysis of the $\nu_{sym}CH_2$ band, the structural role of PG molecules and their level of unsaturation have been documented on genetically manipulated tobacco plants. According to our FTIR data, PG is in intimate contact with the membrane proteins, it provides the proper dynamics of the lipid environment for the functioning of the proteins, but it is not responsible for maintaining their structural stability. It was shown that PG has a structural role which could not have been detected by biochemical methods so far. This structural role provides an explanation for the physiological differences between the wild-type and genetically manipulated tobacco plants.

The results demonstrate the power of systematic analysis of spectroscopic data on model and biological membranes, and that besides applying and rigorously evaluating data of individual spectroscopic techniques, the combination of different methods can provide deeper insight into the investigated phenomena.

Bibliography

[1] Gennis, R. B. (1989) *Biomembranes: Molecular Structure and Function* (Springer-Verlag, New York).

[2] Cevs, G. and Marsh, D. (1987) *Phospholipid Bilayers: Physical Principles and Models* (Wiley-Interscience, New York).

[3] Hazel, J. R. and Williams, E. E. (1990) *Prog. Lipid Res.* **29**, 167–227.

[4] Quinn, P. J. and Williams, W. P. (1983) *Biochim. Biophys. Acta* **737**, 223–266.

[5] Quinn, P. J. and Williams, W. P. (1978) *Prog. Biophys. Mol. Biol.* **34**, 109–173.

[6] Holzenburg, A., Jones, P. C., Franklin, T., Páli, T., Heimburg, T., Marsh, D., Findlay, J. B. C., and Finbow, M. E. (1993) *Eur. J. Biochem.* **213**, 21–30.

[7] Cortijo, M., Alonso, A., Gomez-Fernandez, J. C., and Chapman, D. (1982) *J. Mol. Biol.* **157**, 597–618.

[8] Singer, S. J. and Nicolson, G. L. (1972) *Science* **175**, 720–731.

[9] Killian, J. A., Nicholson, L. K., and Cross, T. A. (1988) *Biochim. Biophys. Acta* **943**, 535–540.

[10] Miller, A.-F. and Brudvig, G. W. (1991) *Biochim. Biophys. Acta* **1056**, 1–18.

[11] Moore, D. J., Sills, R. H., Patel, N., and Mendelsohn, R. (1996) *Biochemistry* **35**, 229–235.

[12] Peticolas, W. L. (1995) *Methods Enzymol.* **246**, 389–416.

[13] Schütz, G. J., Kada, G., Pastushenko, V. P., and Schindler, H. (2000) *Embo J.* **19**, 892–901.

[14] Williams, W. P., Selstam, E., and Brain, T. (1998) *FEBS Lett.* **422**, 252–254.

[15] Cramer, W. A., Whitmarsh, J., and Low, P. S. (1981) *Biochemistry* **20**, 157–162.

[16] Cooley, J. W. and Tukey, J. W. (1965) *Math. Comput.* **19**, 297–301.

[17] Michelson, A. A. (1891) *Philos. Mag.* **31**, 256–259.

[18] Herres, W. and Gronholz, J. (1984) *Comp. Appl. Lab.* **2**, 216–220.

[19] Gronholz, J. and Herres, W. (1985) *Instruments and Computers* **3**, 10–16.

[20] Arrondo, J. L. R., Muga, A., Castresana, J., and Goni, F. M. (1993) *Prog. Biophys. Mol. Biol.* **59**, 23–56.

[21] Siebert, F. (1995) *Methods Enzymol.* **246**, 501–526.

[22] Williams, W. P. and Quinn, P. J. (1987) *J. Bioenerg. Biomembr.* **19**, 605–624.

[23] Shipley, G. G., Green, J. P., and Nichols, B. W. (1973) *Biochim. Biophys. Acta* **311**, 531–544.

[24] Marsh, D. (1991) *Chem. Phys. Lipids* **57**, 109–120.

[25] Casal, H. L. and Mantsch, H. H. (1984) *Biochim. Biophys. Acta* **779**, 381–401.

[26] Mantsch, H. H. and McElhaney, R. N. (1991) *Chem. Phys. Lipids* **57**, 213–226.

[27] Tate, M. W., Eikenberry, E. F., Turner, D. C., Shyamsunder, E., and Gruner, S. M. (1991) *Chem. Phys. Lipids* **57**, 147–164.

[28] Sen, A., Williams, W. P., Brain, A. P. R., and Quinn, P. J. (1982) *Biochim. Biophys. Acta* **685**, 297–306.

[29] Mantsch, H. H., Martin, A., and Cameron, D. G. (1981) *Biochemistry* **20**, 3138–3145.

[30] Tamm, L. K. and Tatulian, S. A. (1997) *Q. Rev. Biophys.* **30**, 365–429.

[31] Cameron, D. G., Casal, H. L., and Mantsch, H. H. (1980) *Biochemistry* **19**, 3665–3672.

[32] Lewis, R. N. A. H., Pohle, W., and McElhaney, R. N. (1996) *Biophys. J.* **70**, 2736–2746.

[33] Moore, D. J. and Mendelsohn, R. (1994) *Biochemistry* **33**, 4080–4085.

[34] Arrondo, J. L. R. and Goni, F. M. (1999) *Prog. Biophys. Mol. Biol.* **72**, 367–405.

[35] Haris, P. I. and Chapman, D. (1992) *Trends Biochem. Sci.* **17**, 328–333.

[36] Surewicz, W. K. and Mantsch, H. H. (1988) *Biochim. Biophys. Acta* **952**, 115–130.

[37] Haris, P. I. and Chapman, D. (1995) *Biopolymers* **37**, 251–263.

[38] Martinez, G. and Millhauser, G. (1995) *J. Struct. Biol.* **114**, 23–27.

[39] Dousseau, F. and Pezolet, M. (1990) *Biochemistry* **29**, 8771–8779.

[40] Lee, D. C., Haris, P. I., Chapman, D., and Mitchell, R. C. (1990) *Biochemistry* **29**, 9185–9193.

[41] Byler, D. M. and Susi, H. (1986) *Biopolymers* **25**, 469–487.

[42] Surewicz, W. K., Moscarello, M. A., and Mantsch, H. H. (1987) *J. Biol. Chem.* **262**, 8598–8602.

[43] Szalontai, B., Nishiyama, Y., Gombos, Z., and Murata, N. (2000) *Biochim. Biophys. Acta* **1509**, 409–419.

[44] Kauppinen, J. K., Moffatt, D. J., Mantsch, H. H., and Cameron, D. G. (1981) *Appl. Spectrosc.* **35**, 271–276.

[45] Kauppinen, J. K., Moffatt, D. J., Cameron, D. G., and Mantsch, H. H. (1981) *Appl. Optics* **20**, 1866–1879.

[46] Kauppinen, J. K., Moffatt, D. J., Mantsch, H. H., and Cameron, D. G. (1981) *Anal. Chem.* **53**, 1454–1457.

[47] Cameron, D. G. and Moffatt, D. J. (1984) *J. Test. Eval.* **12**, 78–85.

[48] Susi, H. and Byler, D. M. (1986) *Methods Enzymol.* **130**, 290–311.

[49] Cameron, D. G. and Moffatt, D. J. (1987) *Appl. Spectrosc.* **41**, 539–544.

[50] Surewicz, W. K., Mantsch, H. H., and Chapman, D. (1993) *Biochemistry* **32**, 389–394.

[51] Jackson, M. and Mantsch, H. H. (1995) *Crit. Rev. Biochem. Mol. Biol.* **30**, 95–120.

[52] van Stokkum, I. H. M., Linsdell, H., Hadden, J. M., Harris, P. I., Chapman, D., and Bloemendal, M. (1995) *Biochemistry* **34**, 10508–10518.

[53] Szalontai, B., Horváth, L. I., Debreczeny, M., Droppa, M., and Horváth, G. (1999) *Photosynth. Res.* **61**, 241–252.

[54] Zhang, H., Ishikawa, Y., Yamamoto, Y., and Carpentier, R. (1998) *FEBS Lett.* **426**, 347–351.

[55] Hadden, J. M., Bloemendal, M., Haris, P. I., Srai, S. K. S., and Chapman, D. (1994) *Biochim. Biophys. Acta* **1205**, 59–67.

[56] Barth, A. (2000) *Prog. Biophys. Mol. Biol.* **74**, 141–173.

[57] McElhaney, R. N. (1986) *Biochim. Biophys. Acta* **864**, 361–421.

[58] Marsh, D. and Horváth, L. I. (1998) *Biochim. Biophys. Acta* **1376**, 267–296.

[59] Morrow, M. R. and Davis, J. H. (1988) *Biochemistry* **27**, 2024–2032.

[60] Surewicz, W. K., Moscarello, M. A., and Mantsch, H. H. (1987) *Biochemistry* **26**, 3881–3886.

[61] Zhang, Y.-P., Lewis, R. N. A. H., Hodges, R. S., and McElhaney, R. N. (1995) *Biophys. J.* **68**, 847–857.

[62] Muga, A., Mantsch, H. H., and Surewicz, W. K. (1991) *Biochemistry* **30**, 7219–7224.

[63] Gasset, M., Mancheno, J. M., Laynez, J., Lacadena, J., Fernández-Ballester, G., del Pozo, A. M., Onaderra, M., and Gavilanes, J. G. (1995) *Biochim. Biophys. Acta* **1252**, 126–134.

[64] Mendelsohn, R., Davies, M. A., Brauner, J. W., Schuster, H. F., and Dluhy, R. A. (1989) *Biochemistry* **28**, 8934–8939.

[65] Haris, P. I., Robillard, G. T., van Dijk, A. A., and Chapman, D. (1992) *Biochemistry* **31**, 6279–6284.

[66] Berliner, L. J. (ed.) (1976) *Spin labeling: Theory and applications* (Academic Press, New York).

[67] Marsh, D. and Horváth, L. I. (1989) In *Advanced EPR. Applications in Biology and Biochemistry*, ed. Hoff, A. J. (Elsevier, Amsterdam). pp. 707–752.

[68] Marsh, D. (1985) In *Spectroscopy and the Dynamics of Molecular Biological Systems*, eds. Bayley, P. M. and Dale, R. E. (Academic Press, London). pp. 209–238.

[69] Boggs, J. M. and Mason, J. T. (1986) *Biochim. Biophys. Acta* **863**, 231–242.

[70] Marsh, D. (2001) *Proc. Natl. Acad. Sci. USA* **98**, 7777–7782.

[71] Fodor, E., Jones, R. H., Buda, C., Kitajka, K., Dey, I., and Farkas, T. (1995) *Lipids* **30**, 1119–1126.

[72] Smirnov, A. I., Smirnova, T. I., and Morse, P. D. (1995) *Biophys. J.* **68**, 2350–2360.

[73] Smirnov, A. I., Belford, R. L., and Clarkson, R. B. (1998) In *Spin Labeling: The Next Millennium*, ed. Berliner, L. J. (Plenum Press, New York). pp. 83–107.

[74] Schneider, D. J. and Freed, J. H. (1989) In *Spin Labeling: Theory and Applications*, eds. Berliner, L. J. and Reuben, J. (Plenum Press, New York). pp. 1–76.

[75] Livshits, V. A. and Marsh, D. (2000) *J. Magn. Reson.* **147**, 59–67.

[76] Kivelson, D. (1960) *J. Chem. Phys.* **33**, 1094–1107.

[77] Griffith, O. H. and Jost, P. C. (1976) In *Spin Labeling: Theory and Applications*, ed. Berliner, L. J. (Academic Press, New York). pp. 453–523.

[78] Páli, T., Kleinschmidt, J. H., Powell, G. L., and Marsh, D. (2000) *Biochemistry* **39**, 2355–2361.

[79] Szidonya, J., Farkas, T., and Páli, T. (1990) *Biochem. Gen.* **28**, 233–246.

[80] Horváth, I., Vigh, L., Páli, T., and Thompson Jr., G. A. (1989) *Biochim. Biophys. Acta* **1002**, 409–412.

[81] Gombos, Z., Kis, M., Páli, T., and Vigh, L. (1987) *Eur. J. Biochem.* **165**, 461–465.

[82] Páli, T., Bartucci, R., Horváth, L. I., and Marsh, D. (1992) *Biophys. J.* **61**, 1595–1602.

[83] Bartucci, R., Páli, T., and Marsh, D. (1993) *Biochemistry* **32**, 274–281.

[84] McConnell, H. M. (1976) In *Spin Labeling: Theory and Applications*, ed. Berliner, L. J. (Academic Press, New York). pp. 525–560.

[85] Kleinschmidt, J. H., Mahaney, J. E., Thomas, D. D., and Marsh, D. (1997) *Biophys. J.* **72**, 767–778.

[86] Páli, T. and Horváth, L. I. (1989) *Biochim. Biophys. Acta* **984**, 128–134.

[87] Horváth, L. I. (1994) *Subcell. Biochem.* **23**, 205–245.

[88] Marsh, D. (1985) In *Progress in Protein-Lipid Interactions*, eds. Watts, A. and de Pont, J. J. H. H. M. (Elsevier, Amsterdam). pp. 143 – 172.

[89] Ivancich, A., Horváth, L. I., Droppa, M., Horváth, G., and Farkas, T. (1994) *Biochim. Biophys. Acta* **1196**, 51–56.

[90] Páli, T., Finbow, M. E., Holzenburg, A., Findlay, J. B. C., and Marsh, D. (1995) *Biochemistry* **34**, 9211–9218.

[91] Knowles, P. F. and Marsh, D. (1991) *Biochem. J.* **274**, 625–641.

[92] de Planque, M. R. R., Greathouse, D. V., Koeppe, R. E., Schäfer, H., Marsh, D., and Killian, J. A. (1998) *Biochemistry* **37**, 9333–9345.

[93] Abadji, V. C., Raines, D. E., Watts, A., and Miller, K. W. (1993) *Biochim. Biophys. Acta* **1147**, 143–153.

[94] Marsh, D. (1999) *Bioscience Rep.* **19**, 253–259.

[95] Sankaram, M. B. and Marsh, D. (1993) In *Protein-Lipid Interactions*, ed. Watts, A. (Elsevier, Amsterdam). pp. 127–162.

[96] Virgin, H. I., Kahn, A., and von Wettstein, D. (1963) *Photochem. Photobiol.* **2**, 83–91.

[97] Sundqvist, C. and Dahlin, C. (1997) *Physiol. Plant.* **100**, 748–759.

[98] Selstam, E. (1998) In *Lipids in Photosynthesis: Structure, Function and Genetics*, eds. Siegenthaler, P. A. and Murata, N. (Kluwer, Dordrecht). pp. 209–224.

[99] von Wettstein, D., Gough, S., and Kannangara, C. G. (1995) *Plant Cell* **7**, 1039–1057.

[100] Reinbothe, S., Reinbothe, C., Lebedev, N., and Apel, K. (1996) *Plant Cell* **8**, 763–769.

[101] Grimm, B., Kruse, E., and Kloppstech, K. (1989) *Plant Mol. Biol.* **13**, 583–593.

[102] Lebedev, N. and Timko, M. P. (1998) *Photosynth. Res.* **58**, 5–23.

[103] Barthélemy, X., Bouvier, G., Radunz, A., Docquier, S., Schmid, G. H., and Franck, F. (2000) *Photosynth. Res.* **64**, 63–76.

[104] Dreyfuss, B. W. and Thornber, J. P. (1994) *Plant. Physiol.* **106**, 829–839.

[105] Reinsberg, D., Booth, P. J., Jegerschold, C., Khoo, B. J., and Paulsen, H. (2000) *Biochemistry* **39**, 14305–14313.

[106] Lee, A. G. (2000) *Curr. Biol.* **10**, R377–R380.

[107] Droppa, M., Horváth, G., Hideg, E., and Farkas, T. (1995) *Photosynth. Res.* **46**, 287–293.

[108] Kruse, O., Hankamer, B., Koczak, C., Gerle, C., Morris, E., Radunz, A., Schmid, G. H., and Barber, J. (2000) *J. Biol. Chem.* **275**, 6509–6514.

[109] Gombos, Z., Várkonyi, Z., Hagio, M., Iwaki, M., Kovács, L., Masamoto, K., Itoh, S., and Wada, H. (2002) *Biochemistry* **41**, 3796–3802.

[110] Murata, N., Sato, N., Takahashi, N., and Hamazaki, Y. (1982) *Plant Cell Physiol.* **23**, 1071–1079.

[111] Murata, N. (1983) *Plant Cell Physiol.* **24**, 81–86.

[112] Bishop, D. G. (1986) *Plant Cell Environ.* **9**, 613–616.

[113] Murata, N. and Yamaya, J. (1984) *Plant Physiol.* **74**, 1016–1024.

[114] Murata, N., Ishizaki-Nishizawa, O., Higashi, S., Hayashi, H., Tasaka, Y., and Nishida, I. (1992) *Nature* **356**, 710–713.

[115] Moon, B. Y., Higashi, S.-I., Gombos, Z., and Murata, N. (1995) *Proc. Natl. Acad. Sci. USA* **92**, 6219–6223.

[116] Leegood, R. C. and Malkin, R. (1986) In *Photosynthetic Energy Transuction: A Practical Approach*, eds. Hipkins, M. F. and Baker, N. R. (Oxford IRL Pess, Oxford). pp. 9–25.

[117] Török, Z., Szalontai, B., Joó, F., Wistrom, C. A., and Vigh, L. (1993) *Biochem. Biophys. Res. Commun.* **192**, 518–524.

[118] Vigh, L., Horváth, I., Joó, F., and Thompson, G. J. (1987) *Biochim. Biophys. Acta* **921**, 167–174.

[119] Henry, E. R. and Hofrichter, J. (1992) *Methods Enzymol.* **210**, 129–192.

[120] Arnon, D. I. (1949) *Plant Physiol.* **24**, 1–15.

[121] Horváth, G., Droppa, M., Hideg, E., and Rózsa, Z. (1989) *J. Photochem. Photobiol. B* **3**, 515–527.

[122] Markwell, M. A. K., Haas, S. M., Tolbert, N. E., and Bieber, L. L. (1981) *Methods Enzymol.* **72**, 296–303.

[123] Folch, J. M., Lees, M., and Sloane, S. G. H. (1957) *J. Biol. Chem.* **226**, 497–509.

[124] Droppa, M., Masojidek, J., and Horváth, G. (1990) *Z. Naturforsch.* **45c**, 253–257.

[125] Bligh, E. G. and Dyer, W. J. (1959) *Can. J. Biochem. Physiol.* **37**, 911–917.

[126] Sigrist, M. and Staehelin, L. A. (1994) *Plant Physiol.* **104**, 135–145.

[127] Krol, M., Ivanov, A. G., Janson, S., Kloppstech, K., and Huner, N. P. A. (1999) *Plant Physiol.* **120**, 193–203.

[128] Humbeck, K., Kloppstech, K., and Krupinska, K. (1994) *Plant Physiol.* **105**, 1217–1222.

[129] Jansson, S. (1994) *Biochim. Biophys. Acta* **1184**, 1–19.

[130] Muga, A., Arrondo, J. L. R., Bellon, T., Sancho, J., and Bernabeu, C. (1993) *Arch. Biochem. Biophys.* **300**, 451–457.

[131] Li, G., Knowles, P. F., Murphy, D. J., Nishida, I., and Marsh, D. (1989) *Biochemistry* **28**, 7446–7452.

[132] Murphy, D. J. (1986) *Biochim. Biophys. Acta* **864**, 33–94.

[133] Marsh, D. (1997) *Eur. Biophys. J.* **26**, 203–208.

[134] Li, G., Knowles, P. F., Murphy, D. J., and Marsh, D. (1990) *J. Biol. Chem.* **265**, 16867–16872.

[135] Jamieson, G. R. and Reid, E. H. (1971) *Phytochemistry* **10**, 1837–1843.

[136] Brentel, I., Selstam, E., and Lindblom, G. (1985) *Biochim. Biophys. Acta* **812**, 816–826.

[137] Selstam, E., Brentel, I., and Lindblom, G. (1990) In *Plant Lipid Biochemistry, Structure and Utilization*, eds. Quinn, P. J. and Harwood, J. L. (Portland Press Limited, London). pp. 39–46.

[138] Williams, W. P. (1998) In *Lipids in Photosynthesis: Structure, Function and Genetics*, eds. Siegenthaler, P. A. and Murata, N. (Kluwer, Dordrecht). pp. 103–118.

[139] Garab, G., Lohner, K., Laggner, P., and Farkas, T. (2000) *Trends Plant Sci.* **5**, 489–494.

[140] Gounaris, K., Brain, A. R. R., Quinn, P. J., and Williams, W. P. (1984) *Biochim. Biophys. Acta* **766**, 198–208.

[141] Thomas, P., Dominy, P., Vigh, L., Mansourian, A., Quinn, P., and Williams, W. (1986) *Biochim. Biophys. Acta* **849**, 131–140.

[142] Mysliwa-Kurdziel, B., Barthelemy, X., Strzalka, K., and Franck, F. (1997) *Plant Cell Physiol.* **38**, 1187–1196.

[143] Szalontai, B., Joó, F., Papp, E., and Vigh, L. (1995) *J. Chem. Soc. Chem. Commun.* **1995**, 2299–2300.

[144] Dluhy, R. A., Mendelsohn, R., Casal, H. L., and Mantsch, H. H. (1983) *Biochemistry* **22**, 1170–1177.

[145] Dluhy, R. A., Moffatt, D., Cameron, D. G., Mendelsohn, R., and Mantsch, H. H. (1985) *Can. J. Chem.* **63**, 1925–1933.

[146] Casal, H. L., Cameron, D. G., Jarell, H. D., Smith, I. C. P., and Mantsch, H. H. (1982) *Chem. Phys. Lipids* **30**, 17–26.

[147] Casal, H. L., Cameron, D. G., Smith, I. C. P., and Mantsch, H. H. (1980) *Biochemistry* **19**, 444–451.

[148] Ariizumi, T., Kishitani, S., Inatsugi, R., Nishida, I., Murata, N., and Toriyama, K. (2002) *Plant Cell Physiol.* **43**, 751–758.

Acknowledgements

This work was performed at the Institute of Biophysics, Biological Research Centre, Hungarian Academy of Sciences.

I am greatly indebted to Professor Pál Ormos, head of the Institute, for providing me with the opportunity to work at the Institute.

I would like to express my warmest thanks to my supervisors, Dr. Balázs Szalontai and Dr. Tibor Páli, head of the group, for their guidance of my work, their inspiring ideas, useful advice and criticism.

I am especially grateful to Professor László I. Horváth for his kind help in ESR spectroscopy.

I am very grateful to Professor Magdolna Droppa and Professor Gábor Horváth for their fruitful cooperation.

My special thanks are due to Professor Derek Marsh for his useful discussions on ESR and FTIR spectroscopy.

I owe very much to my colleagues, my friends and my family for creating all the circumstances enabling me to carry out this work.

Annex